## Versatile Colloidal Syntheses of Metal Chalcogenide Nanoparticles from Elemental Precursors using Amine-Thiol Chemistry

Swapnil D. Deshmukh, † Ryan G. Ellis, † Dwi S. Sutandar, David J. Rokke, and Rakesh Agrawal\*

Davidson School of Chemical Engineering, Purdue University, West Lafayette, IN 47907, USA

† These authors contributed equally

\*Corresponding Author: agrawalr@purdue.edu

#### **Abstract**

Colloidal metal chalcogenide nanoparticles have emerged as a promising hydrazine-free route for the fabrication of solution processed electronic devices. While a wide variety of synthetic pathways have been developed for these nanomaterials, typical colloidal syntheses rely on the use of metal salts as precursors, which contain anionic impurities such as halides, nitrates, acetates, etc. that may incorporate and alter the electrical properties of the targeted nanoparticles. In this report, the recent advances in amine-thiol chemistry, and its unique ability to dissolve pure metals, chalcogens, and metal chalcogenides, is expanded upon for the fabrication of metal chalcogenide nanoparticles. Alkylammonium metal thiolate species are easily formed upon addition of monoamine and dithiol to elemental Cu, In, Ga, Sn, Zn, Se, or metal chalcogenides such as Cu<sub>2</sub>S and Ag<sub>2</sub>S. These species were then used directly for the synthesis of colloidal nanoparticles without the need for any additional purification. The thermal decomposition pathway of one such representative alkylammonium metal thiolate species was studied, verifying that only metal chalcogenides and volatile byproducts are formed, providing a flexible route to compositionally uniform, phase pure, and anionic impurity-free colloidal nanoparticles. Synthetic methods were developed from these precursors to yield pure phase colloidal nanoparticles of binary, ternary, and quaternary materials and their alloys including In<sub>2</sub>S<sub>3</sub>, (In<sub>x</sub>Ga<sub>1</sub>x)2S3, CuInS2, CuIn(SxSe1-x)2, Cu(InxGa1-x)S2, Cu2ZnSnS4, and AgInS2. Successful synthesis with various experimental methods such as heat up, hot injection, and microwave assisted solvothermal reactions were also demonstrated, showing the flexibility and greater scope for this new synthesis route.

#### Introduction

The synthesis of colloidal nanoparticles derived from non-toxic metal chalcogenides is an appealing method of fabricating solution processed electronic devices such as photovoltaics. Solution processing holds the potential to substantially reduce the manufacturing costs of thin film photovoltaics through high throughput, atmospheric pressure processing, high materials utilization, and roll-to-roll compatible deposition over large areas. As such, Cu(In,Ga)(S,Se)<sub>2</sub>, or CIGSSe, and its earth abundant analog Cu<sub>2</sub>ZnSn(S,Se)<sub>4</sub>, or CZTSSe are of particular interest for the fabrication of p-type absorber layers in photovoltaic applications. CIGSSe based photovoltaics have demonstrated high power conversion efficiencies up to 23.35%. Solution processing of these metal chalcogenide materials has shown significant promise, with molecular precursor based approaches reaching certified power conversion efficiencies up to 17.3% for CIGSSe<sup>2</sup> and 12.6% for Cu<sub>2</sub>ZnSnSe<sub>4</sub>.<sup>3</sup> However, both of these solution-processed high efficiency devices are fabricated from hydrazine solvent systems which limits the prospects for scalability due to the solvent's highly explosive and carcinogenic nature. In the past decade, a variety of hydrazine-free inks have been developed for the solution processing of CIGSSe and CZTSSe photovoltaics. Notably, various molecular precursor approaches have emerged making use of metal salts and thiourea in DMSO/DMF, 4-6 aqueous based spray pyrolysis approaches,<sup>7</sup> and metal precursors including metal salts,<sup>8,9</sup> metal chalcogenides,<sup>10,11</sup> and pure metals<sup>10–12</sup> in reactive amine-thiol co-solvents. Similarly, colloidal nanoparticles dispersed in non-polar solvents have been explored as another low-toxicity approach to solution processing of thin films. Of these reported approaches, the colloidal nanoparticle approach has reached promising conversion efficiency of 15% for CIGSSe photovoltaics (a current record for a hydrazine-free solution processed approach), <sup>13</sup> and efficiencies around 10% for the CZTSSe system and it's alloys<sup>14-16</sup> by utilizing Cu(In,Ga)S<sub>2</sub> (CIGS) and Cu<sub>2</sub>ZnSnS<sub>4</sub> (CZTS) nanoparticles. This colloidal nanoparticle approach is compatible with high mass concentration inks a 200 mg/mL for blade coating<sup>13</sup> and inkjet printing, <sup>17</sup> demonstrating the scalability of the technique.

The synthesis of CIGS, CZTS and other metal chalcogenide nanoparticles typically relies on the use of nonchalcogenide metal salts such as metal acetylacetonates, chlorides, iodides, acetates, nitrates, sulfates, oxides, hybrid salts such as Sn(acac)<sub>2</sub>Br<sub>2</sub>, and various hydrate derivatives. <sup>18–24</sup> While careful selection of the salt can tune the reactivity in colloidal synthesis, a drawback to this approach is the presence of anionic impurities which can potentially introduce contaminant elements. In the case of chlorides, Kar et al. observed a distinct C-Cl bond stretch in FTIR, a result of the oleylamine solvent/ligand interaction with chlorine in solution.<sup>25</sup> Such chlorine impurity in CIGSSe photovoltaic device can act as an n-type dopant, influencing the device performance.<sup>26</sup> Similar impurities have been observed in molecular precursors making use of metal halide salts where Murria et al. observed presence of chlorine in organometallic complexes in the solution as well as in the resultant thin films.<sup>27</sup> The highest efficiency CIGSSe photovoltaics fabricated from nanoparticles have made use of acetylacetonates salts in place of chloride salts.<sup>13</sup> However, in the case of indium acetylacetonate and acetate, it has been shown that the heat up in the absence of a sulfur source in oleylamine yields indium oxide. The formation of an oxide phase, especially in the case of the extremely stable, high bandgap gallium oxide, can significantly hinder photovoltaic performance.<sup>29</sup> Along with direct reactions with metals or metal chalcogenides, these anionic impurities can also bind to the nanocrystal surface as a covalently bonded X-type ligand to passivate cationic dangling bonds, which necessitates their removal by post synthesis meta-thesis type ligand exchange processes.<sup>30</sup>

The development of single source organometallic precursors has been explored in colloidal nanoparticle synthesis which can avoid the presence of anionic impurities described in the latter case. Metal dithiocarbamates and xanthates have been explored for the synthesis of CuInS<sub>2</sub> (CIS),<sup>31</sup> CIGS,<sup>32</sup> and CZTS<sup>33</sup> molecular precursors and nanoparticles. However, most of these syntheses involve either the use or the formation of water molecules which requires its complete removal from the product to avoid the formation of metal oxides at higher reaction temperatures during nanoparticle syntheses. Another limitation of this system is the difficulty in forming the selenium containing analogs of xanthates and thiocarbamates for selenide nanoparticle synthesis which requires the use of highly toxic carbon diselenide.<sup>34</sup> Along with these, various other complex organometallic single source precursors have also been explored, which include (PPh<sub>3</sub>)<sub>2</sub>CuIn(SPh)<sub>4</sub>, (TOP)<sub>3</sub>CuIn(S(n-Pr,t-Bu)<sub>4</sub>, (Ph<sub>3</sub>P)<sub>2</sub>Cu(μ-Set)<sub>2</sub>In(SEt)<sub>2</sub>, (Ph<sub>3</sub>P)<sub>2</sub>Cu(μ-Set)<sub>2</sub>Ga(SEt)<sub>2</sub> etc.<sup>21</sup> However, these precursors suffer from more complex synthetic pathways and cannot be synthesized in-situ for large-scale synthesis. There has been a limited exploration into the synthesis of CIGS and CIGSe nanoparticles using pure metals and chalcogens in ethylenediamine via solvothermal synthesis routes. The mechanism for these syntheses relies on the reaction of the immiscible liquid metals (In and Ga) with dissolved copper and selenium, resulting in polydispersed (30-80 nm) and colloidally unstable nanoparticles<sup>35,36</sup> which severely limit the prospects of this synthetic method being employed for solution processed device fabrication.

Recently, amine-thiol chemistry has emerged as a versatile system with the unprecedented ability to dissolve various metal precursors including metal salts, <sup>8,9</sup> pure metals, <sup>10–12</sup> chalcogens, <sup>37–39</sup> and metal chalcogenides <sup>10,11</sup> at relatively high concentrations. These systems have been used to deposit thin films of various metal chalcogenide materials. Although these systems have demonstrated promising performances for CIGSSe and CZTSSe thin film photovoltaic devices, deposition of thin films using this solvent mixture has various issues due to high reactivity, air sensitivity, and highly corrosive nature. Amine-thiol chemistry has largely focused on molecular precursor formation with extremely limited reports of nanoparticle synthesis making use of the chemistry. Amine-thiol chemistry has been used for the synthesis of limited chalcogenide nanoparticles such as lead chalcogenides, Cu<sub>2</sub>ZnSnSe<sub>4</sub>, and CuInSe<sub>2</sub>, however, non-chalcogenide metal salts were still used as cation precursors. <sup>38,40</sup> To date, there is only one report of elemental metals in amine-thiol solutions used for colloidal chalcogenide nanoparticle synthesis, applied by our group to synthesize binary ZnSe nanoparticles. <sup>41</sup>

In this report, the benefits from the amine-thiol based molecular precursor approach and colloidal nanoparticle based approach are combined, yielding an extremely versatile synthetic pathway for colloidal metal chalcogenide nanoparticle synthesis. Amine-thiol chemistry is employed to solubilize elemental metals, chalcogens, and metal chalcogenides to create reactive metal thiolate precursors. These metal thiolate precursors are free of any of the aforementioned anionic (halide, acetylacetonate, acetate, etc.), oxide, and moisture impurities, and can be used directly without the need for additional separation or purification of the precursor solutions. In this report, the versatility of the system is demonstrated through the synthesis of a variety of binary, ternary, and quaternary photovoltaic relevant nanoparticles including In<sub>2</sub>S<sub>3</sub>, (In<sub>x</sub>Ga<sub>1-x</sub>)S<sub>3</sub>, CuInS<sub>2</sub>, CuIn(S<sub>x</sub>Se<sub>1-x</sub>)<sub>2</sub> (CISSe), Cu(In<sub>x</sub>Ga<sub>1-x</sub>)S<sub>2</sub>, Cu<sub>2</sub>ZnSnS<sub>4</sub>, and AgInS<sub>2</sub>. The reactive metal thiolates were thermally decomposed in the coordinating solvent oleylamine to form colloidally stable, phase pure nanoparticles. The flexibility in the experimental synthetic method was also demonstrated by the synthesis of phase pure nanoparticle via hot injection, heat up, and microwave assisted solvothermal reactions. Additionally, in the case of sulfide nanoparticles, no additional sulfur source was used due to the presence of covalent bonds between the metal center and sulfurs in the metal thiolate precursors, eliminating rapid sulfur-metal intermixing concerns present in other synthetic methods. <sup>15</sup> Phase purity, compositional uniformity, morphology, size and ligand

moiety for these particles were investigated by a wide variety of analytical techniques such as XRD, Raman, XRF, TEM, STEM-EDS, <sup>1</sup>H-NMR, and FTIR. The decomposition pathway of these precursors is further investigated via GC-MS and XRD analysis which demonstrates the decomposition of metal thiolates into metal sulfides along with few non-contaminating volatile byproducts. Additionally, the control over size and phase of the particles was demonstrated through variation of reaction conditions, allowing for tailoring of nanoparticles for specific applications.

#### **Experimental Section**

*Materials:* Ga pellets (6 mm dia, 99.99999% metals basis) were purchased from Alfa Aesar. Cu (40-60 nm, >99.5% metal basis with 2% oxygen), In (100 mesh, 99.99% metal basis), Zn (<50 nm, >99% metal basis), Sn (<150 nm, >99% metal basis), Se (100 mesh, 99.99% metal basis), Cu<sub>2</sub>S (powder, 99.99%), Ag<sub>2</sub>S (powder, 99.99%), n-propylamine (PA, 99%), n-octylamine (OA, 99%), 1,2-ethanedithiol (EDT, >98%) and oleylamine (OLA, 70%, primary amines >98%) were purchased from Sigma-Aldrich. All chemicals were used as received except for Ga pellets and oleylamine. The Surface oxide was removed from as-received gallium pellets using a blade and oleylamine was degassed via successive freeze pump thaw cycles prior to use.

Precursor solution preparation: All precursor inks for hot injection and heat up nanoparticle syntheses were prepared by dissolving pure metals in PA and EDT solution at a mole ratio of PA:EDT=2:1. Metal precursor weighing and solution preparations were performed in a glovebox under an inert atmosphere of nitrogen (oxygen and moisture concentration maintained below 1 ppm). For binary nanoparticle synthesis of indium sulfide, 0.4 M ink was prepared by dissolving indium powder in a PA-EDT solution at room temperature. For In-Ga alloyed binary sulfide nanoparticles, inks were prepared with various mole ratios of In to Ga such that the total concentration of In+Ga was maintained at 0.4 M. Metal dissolutions for CIS, CIGS and CZTS nanoparticle synthesis were performed on a Schlenk line under argon atmosphere at 45°C with constant refluxing for faster dissolution to obtain 0.4 M (Cu based) inks. A Cu:In mole ratio of 0.9 was used for CIS nanoparticles while Cu/(In+Ga) and Ga/(In+Ga) mole ratios of 0.9 and 0.3 were used for CIGS nanoparticle synthesis respectively. In the case of CZTS nanoparticle synthesis, Cu/Sn and Zn/Sn precursor mole ratios were maintained at 1.92 and 1.2 respectively. Inks used for time study aliquot experiments for CIGS nanoparticle syntheses were prepared with Cu concentrations of 0.8 M, keeping the metal ratios constant. Inks prepared for CIS nanoparticle syntheses were further used as a solvent for Se powder dissolution to prepare inks for CISSe nanoparticle syntheses. Precursor inks for microwave assisted solvothermal syntheses of CIS nanoparticles were prepared on a Schlenk line under an argon atmosphere at 65°C in OLA-EDT solution instead of PA-EDT solution with an OLA:EDT mole ratio of 2:1, Cu concentration of 0.2 M, and a Cu:In mole ratio of 0.9. An indium precursor ink for GC-MS analysis was also prepared under Schlenk line using OA-EDT solution with an indium concentration of 0.4 M. For experiments involving metal chalcogenides as starting precursors, inks for CIGS and AgInS2 nanoparticle synthesis were prepared by mixing two solutions prior to reaction; i. Metal chalcogenide ink (Cu<sub>2</sub>S or Ag<sub>2</sub>S) in 2:1 mole ratio of PA:EDT with a metal concentration of 0.8 M, ii. Pure metal inks (In+Ga or In) in 2:1 mole ratio of PA:EDT with a metal concentration of 0.88 M.

Nanoparticle Synthesis: For standard heat up reactions, 1 mL of the metal precursor ink in PA-EDT solution was mixed with 8 mL of OLA in a 3 neck flask assembly and then heated to desired reaction temperature (285°C for In<sub>2</sub>S<sub>3</sub>, (In<sub>x</sub>Ga<sub>1-x</sub>)<sub>2</sub>S<sub>3</sub>, CIGS and 250°C for CIS, CISSe, CZTS) under a flowing argon atmosphere on a Schlenk line. A condenser with cooling water was used to reflux the reaction mixture until ~150°C, above which, the cooling water was disconnected for the duration of the reaction to reduce reflux and remove excess PA-EDT from the reaction mixture. The duration of the reaction was measured once the reaction mixture reached the setpoint temperature. CIGS aliquot experiments were performed through this heat up procedure using 30 mL of OLA and 3 mL of 0.8 M (Cu based) ink. For this experiment, once the reaction mixture reached 285°C, samples were collected over the course of the reaction (0 hr, 0.5 hr, 1 hr, 3 hr, 6 hr, 12 hr, and 24 hr) by removing 2 mL of reaction mixture at 285°C using a glass syringe with a stainless steel needle and then quenching it in 5 mL OLA maintained at room temperature.

The standard hot injection reaction for nanoparticle synthesis was performed by heating up 2 solvents separately. Reaction solvent i.e. OLA (8 mL) was heated to desired reaction temperature in 3 neck flask assembly while the metal precursor ink in PA-EDT (1.5 mL) diluted with an equal volume of OLA (1.5 mL) was heated to  $45^{\circ}$ C in a one-neck flask sealed with a rubber septum. Once both the mixtures reached the set temperature, 2 mL of metal precursor ink was quickly injected in hot OLA and then the reaction was continued for the desired duration. Similar to heat up process, the cooling water used for reaction reflux was removed after injection to remove the excess quantities of PA-EDT solvents. The time study on  $In_2S_3$  nanoparticle synthesis was performed using hot injection approach with aliquots at t = 5 min, 1 hr, 6 hr, and 18 hr collected in the manner similar to the CIGS heat up experiment.

For the microwave assisted solvothermal reaction route, 1 mL of 0.2 M (Cu based) CIS-OLA-EDT ink was diluted to 5 mL with OLA and sealed with a crimped PTFE coated silicone septa cap on a 5 mL borosilicate glass microwave

reactor with magnetic PTFE stir bar. The reaction was carried out for 15 min at 225°C with a stirring rate of 600 rpm using a Biotage Initiator EXP 400W microwave reactor.

All particles formed through heat up, hot injection, or microwave assisted solvothermal route were washed using the same procedure. The cooled reaction mixture was transferred to a centrifuge tube and was centrifuged at 14000 rpm for 5 min using isopropanol as an antisolvent. The supernatant from this process was discarded and the precipitated particles were re-dispersed in hexanes. This process was repeated 3 times to remove excess OLA from the nanoparticles. Finally, the nanoparticles were dried under argon flow to remove residual washing solvents and then stored in an inert atmosphere for further analysis.

*Material Characterization:* X-ray diffractograms (XRD) were obtained using a Rigaku Smart Lab diffractometer in Parallel-Beam mode, using a Cu Kα ( $\lambda$  = 1.5406 Å) source operating at 40 kV/44 mA. Transmission electron microscopy (TEM) images were collected using Tecnai G2 20 TEM with an accelerating voltage of 200 kV. STEM-EDS data were collected on Talos 200X TEM containing four silicon drift detectors using SiN grid. Atomic force microscopy was performed using digital instruments multimode atomic force microscope with a IIIa controller under contact mode. Absorption data for particles were collected using the Agilent Cary 60 UV-Vis Spectrophotometer in transmission mode on soda lime glass substrate. Raman spectra were collected on a Horiba/Jobin-Yvon HR800 microscope with an excitation laser wavelength of 632.8 nm. FTIR spectra were collected on Thermo-Nicolet Nexus 670 FTIR unit in transmission mode using NaCl crystal substrates. <sup>1</sup>H-NMR spectra were collected using a Bruker AV-III-400-HD instrument and deuterated chloroform as a nanoparticle dispersing solvent along with ethylene carbonate as a NMR standard. Bulk nanoparticle composition was analyzed using a Fisher XAN 250 X-ray fluorescence (XRF) instrument at 50 kV voltage with primary Ni filter containing silicon drift detector. Gas chromatography mass spectrometry was performed using Agilent 5975C MSD (mass selective detector) equipped with a 7890A gas chromatograph. The column used during this analysis was a DB-5MS 30m x 0.25mm x 0.25mm film. The full scan EI spectra were obtained from 30-400 amu.

#### **Result and Discussion**

#### Synthesis of CIS Nanoparticles:

The synthesis of nanoparticles from elemental metals using amine-thiol chemistry proceed under two regimes, metal thiolate formation and their thermal decomposition to metal chalcogenides. The formation of metal thiolate species takes place via the reaction of a metal with an amine-thiol solution. Our group has reported elsewhere the solution chemistry of elemental indium and copper after reactive dissolution with a monoamine and dithiol solution.<sup>42</sup> The species formed from these dissolutions were identified as an alkylammonium bis(1,2-ethanedithiolate) indium (III) complex and alkylammonium high nuclearity copper (I) thiolate clusters in the case of indium and copper dissolutions respectively. These species have shown high solubility in the bulk amine-thiol solution, making a homogenous precursor that does not require any additional purification. Traditionally, a mixture of ethylenediamine and ethanedithiol is used for the dissolution of pure metals and subsequent fabrication of thin film metal chalcogenides. However, in this work a mixture of propylamine and ethanedithiol is used for pure metal dissolution due to propylamine's higher volatility as compared to ethylenediamine (ethylenediamine b.p. 116°C, propylamine b.p. 47.8°C), allowing for better removal through volatilization during high temperature nanoparticle synthesis. This prevents short chain ligands from binding, which may compromise colloidal stability. For CIS nanoparticle synthesis, copper and indium were dissolved together in PA-EDT solution as described in the experimental section. The completion of metal thiolate formation was indicated by disappearance of metal powders and a color change to a clear pale yellow/orange solution. In the second regime, the dissolved metal thiolates were thermally decomposed in the presence of a coordinating solvent to create a colloidally stable nanoparticle suspension. Oleylamine was selected as the coordinating solvent for reaction due to its wide use in colloidal syntheses of copper based metal chalcogenide nanoparticles.<sup>21</sup> Oleylamine's high boiling point of ~350°C and excellent thermal stability allow for high temperature synthesis. Additionally, its long carbon chain length affords excellent colloidal stability through steric hindrance between nanoparticles while strongly coordinating to the nanoparticle surface via the nitrogen lone pair on the amine. 43

Hot injection is a commonly used approach for the synthesis of CIS nanoparticles. <sup>18,21</sup> The hot injection approach was explored using the procedure described in the experimental section whereby the metal thiolate precursor diluted with OLA was injected into preheated OLA. After a swift injection, the reaction was held at 250°C for a duration of one hour followed by natural cooling. Purified particles were obtained from this reaction mixture following a particle washing process as explained in the experimental section. The XRD spectrum for synthesized particles is shown in Figure 1a, confirming the formation of CIS material. The absence of any binaries was further confirmed via Raman analysis (Figure S1) and an average particle size of around 6-8 nm was observed from the TEM image of these particles (Figure 1b). The traditional hot injection method is generally considered to suffer from poor scalability due to mixing concerns in high volume reactions, and irreproducibility concerns from the injection itself. These concerns are largely

mitigated while using the developed amine-thiol approach. Especially, the intermixing of separate metal cation and sulfur solutions is eliminated due to the covalently bonded metal centers with sulfur atoms in the metal thiolate precursors.

Despite the success with this improved hot injection route, the reaction conditions like the local concentration at the point of injection and the impact it has on ligand coordination may affect the reaction kinetics as the result of mixing dynamics. An alternative experimental technique that is widely considered more scalable than the hot injection method is a one pot heat up method, which has demonstrated easily scaled reactions with greater than gram scale syntheses of metal chalcogenide nanoparticles. To study the one pot heat up synthesis of CIS nanoparticles using amine-thiol precursors, reaction parameters were chosen as described in the experimental section. Unlike hot injection experiments for CIS nanoparticles where the CIS precursor is exposed to high temperature (250°C) very rapidly resulting in immediate nucleation of nanoparticles, the heat up process exposes the precursor solution to various increasing temperatures over a much longer time scale. During this heat up process, the initially clear pale yellow/orange reaction mixture turned transparent dark yellow at around 120°C and at approximately 140°C, the reaction mixture turned dark brown/black suggesting the nucleation of nanoparticles. The reaction was ramped to 250°C and maintained at this temperature for 1 hour. Although this approach is suitable for large scale batch reactions, it tends to form slow-toconsume binary phases at temperatures below the reaction dwell temperature and affect the properties of synthesized particles.<sup>34</sup> However, the resultant XRD spectrum (Figure 1) and Raman spectrum (Figure S1) for synthesized particles confirm formation of CIS material without any binary phases with average particle size in the range of 6-8 nm, similar to that of hot injection method (Figure 1b).

Another scalable synthetic method based on heat up principles is microwave assisted solvothermal reaction which was utilized to demonstrate flexibility in nanoparticle synthesis routes from amine-thiol precursor solutions. To avoid the over pressurization of the reaction vessel, a metal precursor ink for this reaction was formulated using OLA-EDT instead of PA-EDT as described in the experimental section. Due to the equipment limitation, the reaction was carried out at slightly lower temperature (i.e. 225°C instead of 250°C) for 15 min, resulting in smaller particle sizes (< 5nm) as can be seen from Figure 1b. The XRD for these particles (Figure 1a) show a broader peak at 27.9° with the absence of a peak near 32.3° when compared to heat up and hot injection particles. This variation in XRD spectrum could result from increased FWHM due to smaller particle size or formation of wurtzite phase CIS, possibly due to the different reaction conditions such as lower initial thiol volume, high pressure, rapid heating, retention of volatile species (notably thiols), etc. The Raman spectrum of these particles also supports formation of CIS but with reduced crystallinity observed from peak broadening for A1 mode of CIS particles at 294 cm<sup>-1</sup> (Figure S1).

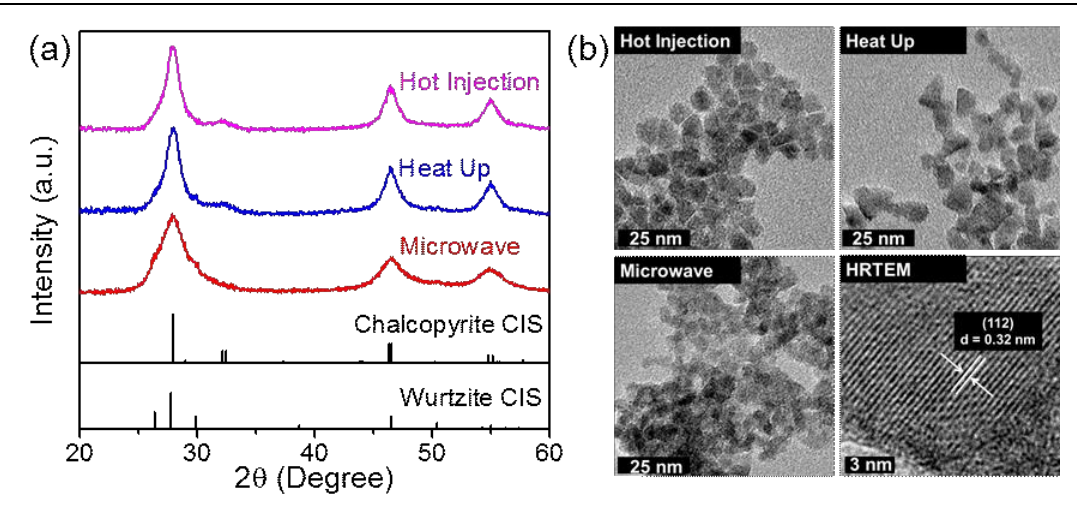


Figure 1. (a) XRD analysis and (b) TEM images of CIS nanoparticles synthesized using hot injection, heat up and microwave assisted solvothermal reactions. HRTEM image on bottom right corresponds to heat up synthesized CIS nanoparticles. (Chalcopyrite and wurtzite phase CIS standards with ICSD collection code 186714 and 163489 respectively)

#### Metal Thiolate Decomposition Mechanism to Metal Chalcogenide Nanoparticles:

The dissolution of metals in amine-thiol solutions have shown to form metal thiolate species which break upon heating to metal chalcogenide materials. Unlike CIS which has little to no solubility in amine-thiol solutions, binary

chalcogenides including In<sub>2</sub>S<sub>3</sub>, Cu<sub>2</sub>S, and CuS have reasonable solubility in amine-thiol solutions. This may suppress the nucleation of binary chalcogenides in the presence of ethanedithiol and oleylamine at temperatures below ethanedithiol's boiling point of 146°C, resulting in phase pure CIS nanoparticle synthesis. To understand the thermal decomposition mechanism of metal thiolates into metal chalcogenides, the exposure of an individual metal thiolate species to higher temperatures was investigated. This can be done by performing a reaction of either Cu or In thiolate at higher temperatures to form copper sulfide or indium sulfide respectively. As the indium thiolate complex in an amine-thiol solution is well defined, it was chosen to study the reaction mechanism and the effect of amine-thiol solvents on nucleation of binary metal chalcogenides.

The synthesis of binary indium sulfide was carried out at 285°C via the hot injection route as described in the experimental section. Immediate injection of the In-PA-EDT (diluted in OLA) ink in preheated OLA resulted in a vibrant yellow color suspension suggesting the formation of indium sulfide particles. Aliquots at different time intervals (5 min, 1 hr, 6 hr, and 18 hr) were collected for analysis after injection of the precursor ink. The XRD spectra collected on the particles obtained after purification are shown in Figure 2a. The first aliquot taken 5 minutes after injection shows broad XRD peaks, indicative of the low crystallinity of the formed material. The peak centered at a 20 of 19.5° matches closely to the trigonal crystal structure of In<sub>1.95</sub>S<sub>3</sub>. Subsequent aliquots show the conversion of trigonal crystal structure to tetragonal In<sub>2</sub>S<sub>3</sub> crystal structure with complete phase purity achieved after maintaining the mixture at the reaction temperature for 18 hours. Compared to the ICSD standard for In<sub>2</sub>S<sub>3</sub>, the XRD spectrum of synthesized material shows different relative peak intensities which suggest a relatively different crystal orientation in the synthesized material.

Along with phase evolution with time, the indium sulfide nanoparticles formed via this route also show structural evolution from amorphous nano-wire-like structures (5 min reaction) to crystalline faceted 2D nano-sheet-like structures (18 hr reaction) as shown in Figure 2b. The conversion of  $In_{1.95}S_3$  to  $In_2S_3$  over 18 hours is suspected to be an effect of ethanedithiol quantity in the solution, while the increasing crystallinity could be attributed to the longer annealing times at the reaction temperature. It is hypothesized that the removal of ethanedithiol (which can act as a sulfur source during the reaction), due to boiling off from continuous heating at  $285^{\circ}$ C, could drive the sulfur reduction in the trigonal crystal structure resulting in tetragonal  $In_2S_3$ . This hypothesis was verified by injecting an indium ink with a reduced EDT quantity, prepared using PA:EDT mole ratio of 11:1 instead of 2:1, into OLA at  $285^{\circ}$ C. This injection resulted in a mixture of  $In_{1.95}S_3$  and  $In_2S_3$  after one hour of reaction with a relatively higher quantity of  $In_2S_3$  as compared to the previous indium sulfide synthesis (Figure S2), specifying the role of thiol quantity on the phase of indium sulfide particles.

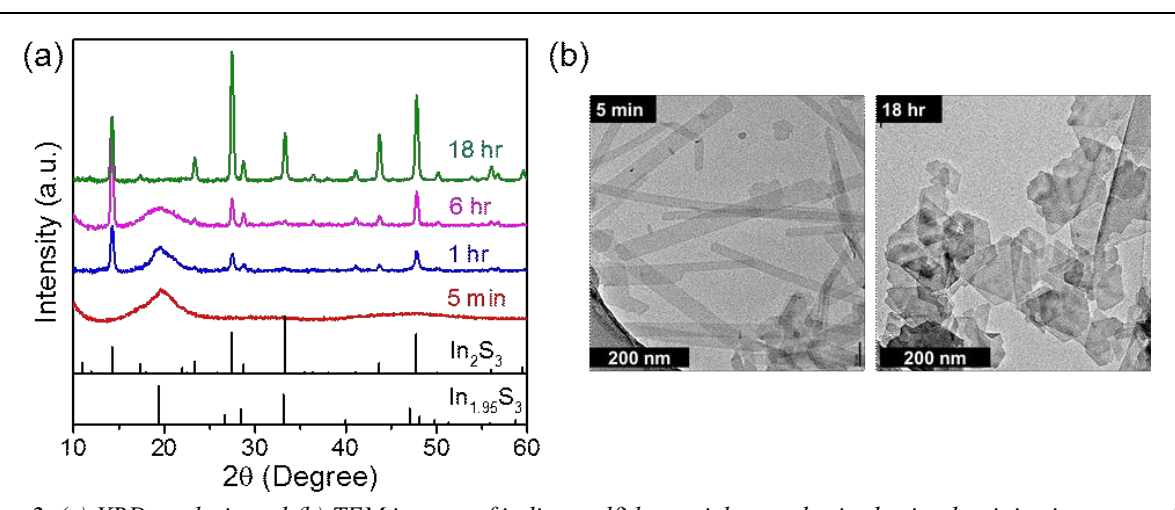


Figure 2. (a) XRD analysis and (b) TEM images of indium sulfide particles synthesized using hot injection route with different time aliquots showing amorphous to crystalline transition with time. (Tetragonal phase  $In_2S_3$  and trigonal phase  $In_{1.95}S_3$  standards with ICSD collection code 151645 and 244280 respectively)

The effect of thiol quantity and its role in the formation of phase pure  $In_2S_3$  was further exploited to understand the complete reaction pathway for converting metal thiolate species to metal chalcogenides. For this purpose, a microwave assisted solvothermal route, which has the ability to contain all the reaction products and byproducts in one sealed vessel, was used. The indium ink used for this reaction was prepared in OA-EDT mixture instead of PA-EDT mixture to maintain comparatively low pressure in the sealed reaction vessel when heating to 200°C. The amount of

ethanedithiol used for the indium precursor preparation was the minimum required amount for dissolution according to the stoichiometry discussed by Zhao et al. to form phase pure In<sub>2</sub>S<sub>3</sub> and to avoid binary redissolution after reaction completion. This reaction was carried out for 15 min at 200°C via microwave heating followed by natural cooling to room temperature. The reaction mixture was then centrifuged in an inert atmosphere without the addition of an antisolvent to precipitate indium sulfide nanoparticles from solution. The supernatant obtained from this separation was analyzed using GC-MS to identify liquid and dissolved gas byproducts formed during the metal thiolate thermal decomposition. Octylamine, with an elution time of 11 minutes in the GC column, was a major component in the reaction mixture. To avoid its domination in GC spectra, the sample was analyzed up to a 10 min elution time. Results obtained from this analysis are presented in Figure S3, showing three peaks in the GC spectrum at elution times of around 1.35 min, 2.1 min and 6.1 min. After analysis in the mass spectrometer, the peaks were assigned to H<sub>2</sub>S, thiirane, and 1,2-ethanedithiol respectively. Based on the indium thiolate structure proposed by our group for an indium-hexylamine-ethanedithiol solution<sup>42</sup> in conjunction with the GC-MS analysis of reaction products, a balanced chemical reaction is proposed in Scheme 1. This reaction demonstrates the clean decomposition of metal thiolate to metal chalcogenide and volatile byproducts that will quickly evaporate from the reaction mixture at high temperature, supporting the use of amine-thiol chemistry for impurity-free metal chalcogenide nanoparticles synthesis.

Scheme 1. Proposed reaction mechanism for indium sulfide synthesis from an alkylammonium indium thiolate species

$$2R - \stackrel{\textcircled{\tiny \$}}{\text{\tiny NH}_3} \left[ \stackrel{\textbf{S}}{\underbrace{\hspace{1cm}}} \stackrel{\textbf{S}}{\text{\tiny NH}_2} \right] \stackrel{\triangle}{\rightarrow} \ln_2 S_3 + 4 \stackrel{\textbf{S}}{\underbrace{\hspace{1cm}}} + H_2 S + 2R - NH_2$$

In the case of ternary CIS nanoparticle synthesis, the copper complex is present alongside the indium complex. The decomposition of the copper-thiolate complex alone in OLA is found to form mixed phase copper sulfide material as verified by XRD (Figure S4). This multiphase copper sulfide formation could be attributed to the presence of variety of copper complexes in Cu-amine-thiol solution as opposed to well-defined single indium complex in In-amine-thiol solution as studied by Zhao et al.<sup>42</sup> Although multiple complexes were proposed for copper (I) thiolates, the structural motif for these structures is similar to the indium thiolate complex. So, it is expected that the copper species also undergo a similar decomposition pathway as indium species giving similar volatile byproducts. It is believed that the co-existence of copper and indium thiolate species in the solution directly nucleates the ternary phase CIS at relatively low temperatures of ~120-140°C, while keeping the binaries dissolved under the boiling point of ethanedithiol, demonstrating a viable reaction pathway to avoid deleterious binary formation.

#### Alloying:

#### In/Ga alloying:

Along with pure metal chalcogenides, alloyed materials formed via metal or chalcogen alloying provide tunability of various optoelectronic properties. In the case of CIS photovoltaics, alloying of indium/gallium, and selenium/sulfur has led to substantial improvements in photovoltaic power conversion efficiencies through bandgap tunability and grading. As such, metal alloying was investigated for the amine-thiol based synthetic methods developed in this report. Alloying was first tested with the incorporation of Ga into indium sulfide nanoparticles. From the available literature, the dissolution of gallium by the amine-thiol route has been possible only in the presence of selenium using diaminedithiol mixtures, limiting the possibility of gallium containing pure sulfide materials. 11 However, in our group's work, it was discovered that gallium could be co-dissolved with indium in a monoamine-dithiol solution without selenium.<sup>44</sup> This enabled the novel preparation of indium gallium sulfide nanoparticles in this work. For these experiments, In+Ga solutions were prepared in PA-EDT mixtures at Ga/(In+Ga) mole ratios of 0.5 (50% Ga) and 0.9 (90% Ga) with a total In+Ga concentration of 0.4 M. A hot injection reaction (as described in the experimental section) was performed using these solutions for a duration of 1 hour at 285°C. XRD analysis of the resulting nanoparticles is presented in Figure S5, showing a shift in trigonal In<sub>2</sub>S<sub>3</sub> peak and the presence of a new broad peak at around 30° suggesting the incorporation of gallium. The XRD obtained with Ga incorporation also shows the reduced crystallinity of the nanoparticles as compared to the pure indium sulfide. This variation is also observed in the particle morphology, where faceted 2D nano-sheet-like structures break down to nano-wire-like structures (Figure S6) with increasing Ga content. The lower crystallinity observed in Ga rich material is in agreement with the literature, as gallium sulfide materials are known to exhibit poor crystallinity, even up to synthesis temperatures of 400°C.<sup>45</sup> The incorporation of Ga in the bulk material was also analyzed using X-ray fluorescence, which confirmed the Ga/(Ga+In) ratio of 0.42 and 0.85 in final material for reactions with starting Ga/(Ga+In) ratio of 0.5 and 0.9 respectively. Although the bulk material showed incorporation of Ga, the amorphous nature of XRD makes it difficult to verify the presence of alloying in the material. The possibility of the formation of two different phases in the reaction, one with amorphous  $Ga_2S_3$  and other with small  $In_2S_3$  particles, cannot be completely ruled out based on the XRD pattern. So, to confirm the indium-gallium alloying, UV-Vis absorption spectroscopy was performed on thin films cast from suspensions of the purified nanoparticles. As the direct bandgap of pure  $In_2S_3$  is ~2.1 eV and that of  $Ga_2S_3$  is ~3.45 eV, the gradual increase observed in optical bandgap of  $(In,Ga)_2S_3$  with increasing Ga content supports the formation of gallium alloyed indium sulfide nanoparticles and eliminates the possibility for discrete  $In_2S_3$  and  $Ga_2S_3$  formation. The homogeneity of Ga incorporation within single nanoparticle was further verified via STEM-EDS mapping of the material containing 50% starting Ga content and is shown in Figure 3b, while the uniformity between multiple nanoparticles is presented in Figure S7. The thickness of one of these particles was observed in the range of 4-6 nm when measured using atomic force microscopy, which confirms the nano-sheet-like nature of this material (Figure S8).

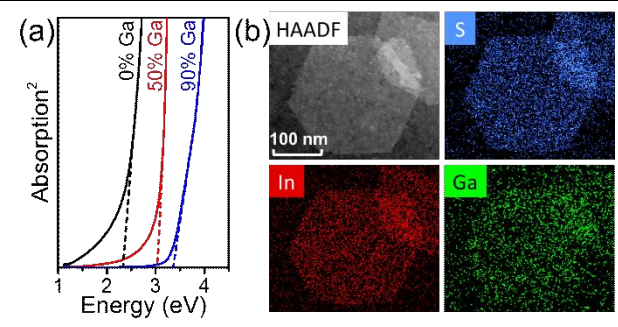


Figure 3. (a) Tauc plot for the data obtained through UV-vis absorption spectroscopy on indium-gallium sulfide nanoparticles with different gallium content. (b) STEM-EDS elemental mapping of indium-gallium sulfide nanoparticles containing 50% Ga.

The successful alloying of gallium into indium sulfide was further applied to the ternary alloy system of CIGS using a one-pot heat up process similar to the aforementioned CIS nanoparticle synthesis. To study the incorporation of gallium and phase purity as a function of temperature, aliquots were collected at temperature intervals of around 25°C starting at 175°C to the final reaction temperature of 285°C. The Raman spectrum of the first aliquot collected at 175°C shows the absence of any binary metal chalcogenides and confirms the formation of CIS (Figure S9, black spectrum). The XRD peak near 20 of 46.5° shows a gradual shift towards higher angle demonstrating the incorporation of Ga into the CIS crystal structure as a function of temperature (Figure 4a). This Ga incorporation was further confirmed by analyzing the bulk composition of purified particles using X-ray fluorescence technique (Figure 4b). While at 175°C, very little gallium had incorporated into the nanoparticles, by 285°C, XRF analysis confirmed that the CIGS nanoparticles achieved the target composition of Ga/(Ga+In) = 0.3. As is consistent in other CIGS synthetic pathways, gallium incorporation indeed requires higher temperatures than CIS nanoparticle formation. However, for this study, aliquots were taken during heat up process with no dwell time at each temperature. Additional dwell time at lower temperatures may provide a route to form the targeted CIGS composition without heating to higher temperatures.

Along with the effects of the gradual increase in reaction temperature on particle composition, the size of the particles was also studied with respect to time. After reaching the reaction temperature of 285°C, aliquots were collected at t = 0 hr, 0.5 hr, 1 hr, 3 hr, 6 hr, 12 hr, and 24 hr. The average nanoparticle size analyzed via transmission electron microscopy (Figure 4c) and XRD (Figure S10) shows a gradual increase in particle size with respect to time, reaching an average particle size of >15nm for the 24 hr reaction. The CIGS particles formed via this amine-thiol route have shapes and size distributions similar to the previously discussed CIS syntheses. While the bulk composition of the synthesized nanoparticles measured by XRF shows that the targeted composition was reached, the elemental uniformity within single particles was analyzed using STEM-EDS. The elemental mapping obtained for 3 hr reaction particles from STEM-EDS analysis of two adjacent particles is shown in Figure S11, which confirms elemental uniformity between two particles as well as within a single particle. The particles were also analyzed via FTIR and

<sup>1</sup>H-NMR techniques, confirming the presence of oleylamine on particle surface acting as a ligand (Figure S12). This provided a stable particle suspension in nonpolar (or very low polarity) solvents like toluene under an inert atmosphere for well over 6 months with no visible settling, exemplifying the excellent colloidal stability of the nanoparticles.

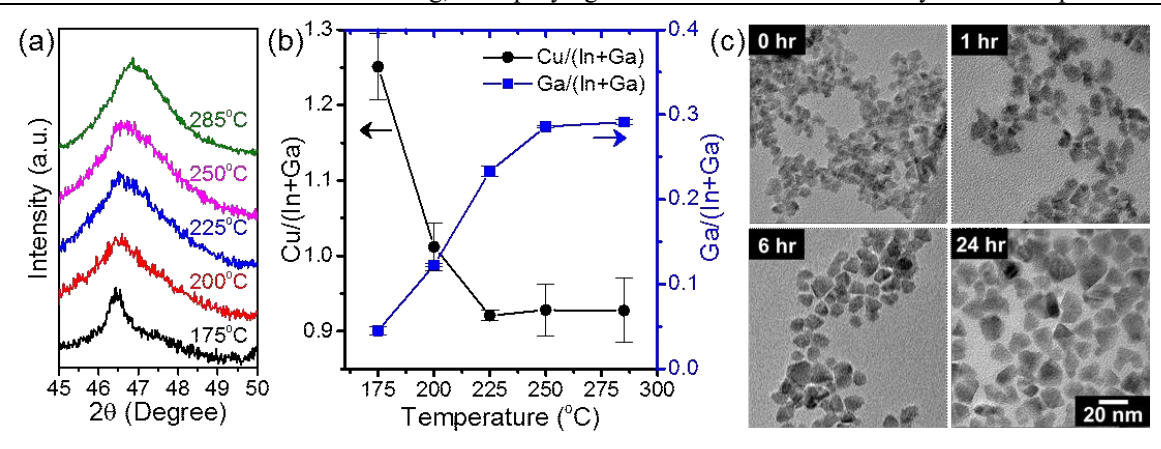


Figure 4. (a) XRD analysis focused on a peak near 20 of 46.5° and (b) Plot summarizing X-ray fluorescence analysis on CIGS nanoparticles showing gallium incorporation as a function of temperature. (c) TEM images of CIGS nanoparticles showing size variation as a function of time

#### S/Se alloying:

Similar to metal alloying, chalcogen alloying of various semiconducting materials also provide tunability in material properties. In the case of CIS, incorporation of Se into the CIS crystal structure reduces the bandgap of the material from 1.5 eV for the pure sulfide to 1.0 eV for the pure selenide. 46 As the amine-thiol solvent system also dissolves pure chalcogens, it provides additional benefits over traditional synthesis routes for metal selenide nanoparticles, 38 which often rely on alkyl-phosphines for dissolution. 18,21 Utilizing the elemental Se dissolution ability of the aminethiol system, CISSe nanoparticles were synthesized through a one pot heat up process. The formation of sulfur-free selenides through the pure metal amine-thiol route is challenging and relies on excess selenium in the reaction mixture due to the covalent bonding between the metal atom and the sulfur in the metal thiolate complex. To study the incorporation of Se in the metal chalcogenide structure, various quantities of Se powder were dissolved in the CIS solution prepared in PA-EDT solvent to obtain Se/(Cu+In) ratios of 0, 0.5, 1, and 2 in the precursor ink. The XRD analysis of synthesized particles is presented in Figure S13 while a representative shift observed in the XRD peak near 20 of 27° (112 plane) shown in Figure 5a, demonstrates the transition of CIS to CISSe with increasing Se quantities. This incorporation of Se studied via Raman analysis is shown in Figure 5b. The disappearance of CIS Raman peaks at around 294 cm<sup>-1</sup> and 340 cm<sup>-1</sup> with increasing Se content in the reaction mixture and the simultaneously increasing intensity of CISe peaks at 180 cm<sup>-1</sup> and 228 cm<sup>-1</sup>, confirms the transition of pure CIS to a sulfur poor CISSe nanoparticles. XRF analysis performed on these particles also supports this trend with Se/(Cu+In) ratios of 0, 0.44, 0.75, and 0.92 obtained for starting Se/(Cu+In) ratios of 0, 0.5, 1, and 2 respectively. The elemental mapping of CISSe nanoparticles with Se/(Cu+In) ratio of 0.92 is shown in Figure S14, which confirms uniform incorporation of Se and the presence of residual S in the particles. It is expected that additional increases in the Se/(Cu+In) ratio in starting precursor will drive the reaction to increasingly pure selenide material. While reaction time was not extensively studied for selenium alloying, longer reaction times may also allow for more complete incorporation of selenium into the synthesized material.

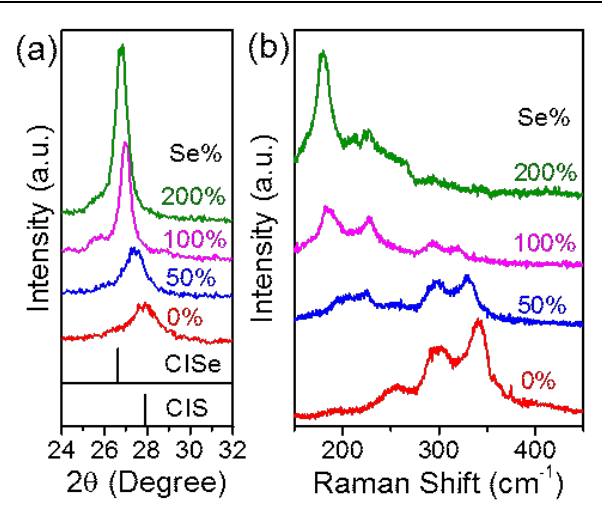


Figure 5. (a) XRD analysis, focused on a peak near 2θ of 27° (Chalcopyrite phase CIS and CISe standards with ICSD collection code 186714 and 73351 respectively) and (b) Raman spectroscopy analysis on CISSe nanoparticles as a function of Se quantity.

#### Versatility of Synthesis Route:

#### **Synthesis of CZTS nanoparticles:**

Due to the high demand and scarcity of indium, the search for earth-abundant metal chalcogenide photovoltaic materials led to the development of the CZTS material system which is analogous to the CIGS system. The chemistry explored for the synthesis of binary indium sulfide, indium gallium sulfide and ternary CIS, CIGS, CISSe was applied to the quaternary system of CZTS as the pure Zn and Sn metals are soluble in the amine-dithiol mixture. A CZTS nanoparticle synthesis was performed via a heat up process as explained in the experimental section. As many traditional syntheses of CZTS material in OLA are carried out at 250°C, the same temperature was chosen for this reaction. The reaction was carried out for a total of 3 hours after the reaction mixture had reached 250°C. After purification, the nanoparticles were analyzed via XRD, Raman, and STEM-EDS analysis. The XRD spectrum collected on these particles confirms the formation of kesterite phase CZTS nanoparticles (Figure 6a). These particles are smaller in size when compared to CIS particles synthesized under similar reaction conditions (Figure 6b). Traditionally, syntheses of CZTS nanoparticles are known to form compositional inhomogeneities with particle size distribution. Various approaches including longer reaction time, size selective particle separation, change in precursor injection sequence etc. were adopted to reduce this inhomogeneity. 15,47,48 Unlike these syntheses, the nanoparticles obtained for the CZTS system using the chemistry in this work show reduced polydispersity suggesting better homogeneity in particle composition, possibly caused due to metal-sulfur covalent bond in the precursor solution. This uniformity is also supported by elemental mapping of CZTS particles obtained via STEM-EDS analysis (Figure S15). Raman analysis performed on these particles also confirm the formation of CZTS material with characteristic peaks observed at 289 cm<sup>-1</sup>, 339 cm<sup>-1</sup> and 374 cm<sup>-1</sup> dominating the spectrum (Figure S15). Due to the very similar Raman spectra of Cu<sub>2</sub>SnS<sub>3</sub> (CTS) and CZTS, and also the presence of a possible minor peak at 356 cm<sup>-1</sup>, the coexistence of a secondary CTS phase in the nanoparticles cannot be ruled out. This secondary phase, if present, is commonly observed for CZTS nanoparticle synthesis.<sup>15</sup>

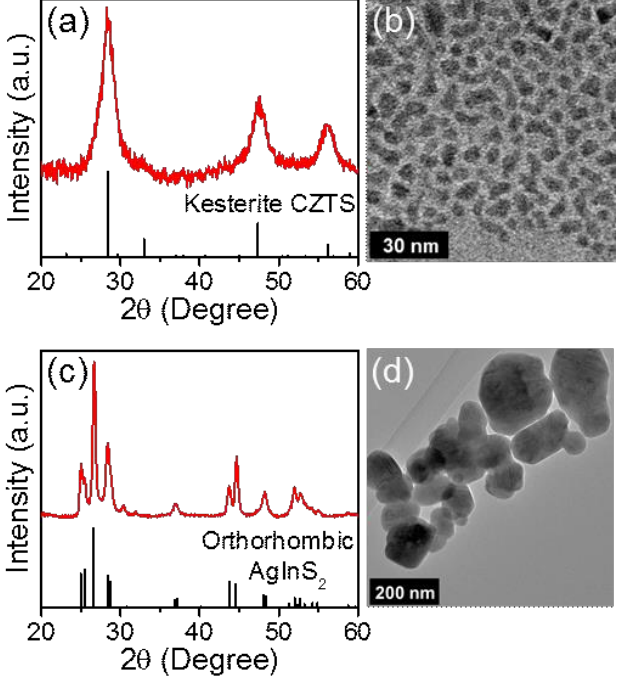


Figure 6. (a) XRD analysis (simulated kesterite phase CZTS standard obtained from JCPDS 26-0575) and (b) TEM image of CZTS nanoparticles. (c) XRD analysis (Orthorhombic phase AgInS<sub>2</sub> standard with ICSD collection code 51618) and (d) TEM image of AgInS<sub>2</sub> nanoparticles.

#### <u>Using Metal Chalcogenide Precursors:</u>

Interestingly, it was found that high purity copper (>3N) was extremely difficult to dissolve, and its dissolution only marginally took place over several weeks in PA-EDT solutions. Typically, nanopowders of copper were used as a feedstock to ensure dissolutions over the course of days as opposed to weeks. However, these as received nanopowders of copper typically contained a small fraction of surface oxide, which is not ideal in the pursuit of impurity-free feedstocks (Figure S16a). It is unclear whether the higher reaction/dissolution rate was purely a function of nanoparticle size or if the small oxide content catalyzed the reaction and is currently the topic of further study. Because metal sulfides are known to be readily soluble in amine-thiol solutions, the copper nanopowder was easily replaced with high purity (4N) copper (I) sulfide, which did not contain any appreciable oxide content (Figure S16b). It was found that copper sulfide was rapidly soluble in propylamine-dithiol mixtures. Higher solubility and higher dissolution rates were observed when Cu<sub>2</sub>S was dissolved separately from In/Ga. The Cu<sub>2</sub>S and In/Ga precursor solutions were mixed after complete dissolution yielding a 0.8M (Cu based) solution of Cu<sub>2</sub>S, In, and Ga complexes. The mixed metal sulfide/pure metal precursor solution was used under identical reaction conditions as the previous CIGS heat up reactions from pure metal precursor solutions. Slightly different reactivity was observed when using copper sulfide as a precursor, with the initial color change from a transparent yellowish solution to a dark blackish brown suspension observed between 90-110°C as opposed to 120-140°C for the pure metal precursor case. It is hypothesized that the additional sulfur in solution from the Cu<sub>2</sub>S precursor as compared to the pure metal case may enhance the net reactivity and may initially form CIS at a lower temperature. XRD and Raman spectra, collected on purified nanoparticles obtained after 3 hr of reaction, as shown in Figure S17, confirm the presence of phase pure chalcopyrite CIGS nanoparticles and the TEM image of these particles also show similar average size compared to nanoparticles synthesized from pure metal precursor inks.

The use of metal sulfides in place of pure metals is also advantageous in the case where the pure metal is insoluble in amine-thiol solutions. This was demonstrated for the synthesis of  $AgInS_2$  nanoparticles. Although there have been reports on co-dissolution of silver with copper, zinc and tin precursors in diamine-dithiol solution, <sup>49</sup> we observed no solubility of pure silver with or without indium in amine-thiol solution. In its place, we find that  $Ag_2S$  can be solubilized in under a minute at room temperature using PA-EDT solutions at a concentration of 0.8M (Ag based).

Synthesis of AgInS<sub>2</sub> was performed by mixing precursor inks of Ag<sub>2</sub>S-PA-EDT and In-PA-EDT. These precursor inks were diluted with OLA and used for a hot injection reaction at 250°C for one hour. The XRD obtained for these particles supports the formation of orthorhombic AgInS<sub>2</sub> system as can be seen from Figure 6c. A very weak diffraction signal observed at 30.3° does not correspond to orthorhombic AgInS<sub>2</sub>, rather it represents a marginal presence of tetragonal phase AgInS<sub>2</sub>. Unlike CIS nanoparticles, the particles obtained for AgInS<sub>2</sub> system are bigger and polydisperse with sizes in the range of 50-200nm (Figure 6d). The effect of various Ag precursors and their corresponding reactivity resulting in diverse as well as larger particle morphology has been studied in a literature<sup>50</sup> which suggests the possibility of greater reactivity of Ag-amine-thiol precursor as compared to traditional Ag salt precursors. Further optimization of reaction conditions such as temperature, time, solvent etc., is required for better control over the size of the particles.

#### Synthesis of Wurtzite Phase CIGS nanoparticles:

While demonstrating the versatility of nanoparticle synthesis through the dissolution of variety metal precursors, this chemistry also provided a route to control the phase of a material via a change in the reaction conditions. As mentioned earlier, microwave assisted route for CIS nanoparticles suggested a possible formation of wurtzite phase which was suspected to be a result of different reaction conditions obtained in microwave assisted synthesis compared to normal heat up or hot injection route. The microwave assisted solvothermal route is in principle similar to heat up route except it has a faster heating rate, higher reaction pressure, and volatile byproducts are retained in the sealed vessel. To identify the role of heating rate in the formation of wurtzite phase material, another heat-up synthesis was carried out for CIGS nanoparticles with a faster heating rate under ambient pressure. The heating rate used during the aliquot experiment in the previous section for chalcopyrite CIGS nanoparticles was on average 4.4°C/min. This rate was changed to an average value of 8.8°C /min and a similar aliquot time study was performed. The XRD analysis (Figure 7) of initial aliquots show similar spectrum to that of microwave assisted CIS nanoparticles with peak broadening at 20 of 28.2° and absence of the peak at 20 of 32.5° (note that these positions are different from CIS peak positions due to the incorporation of Ga). Particles obtained after 18 hours of reaction showed 3 unique sharp peaks near 2θ of 28.2° and a new peak at around 2θ of 50.7°, confirming the formation of wurtzite phase CIGS. TEM image of the 3 hr reaction particles (Figure S18) shows a similar particle size of around 10 nm as compared to 3 hr chalcopyrite CIGS.

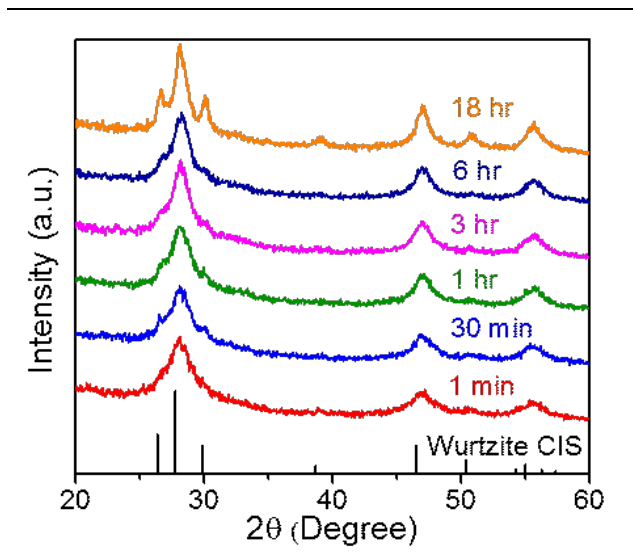


Figure 7. X-ray diffraction analysis on CIGS nanoparticles as a function of time synthesized via heat up synthesis with 8.8°C /min heating rate showing the formation of wurtzite phase. (Wurtzite phase CIS standard with ICSD collection code 163489)

#### Conclusion

In summary, the metal dissolution ability of the reactive amine-thiol solvent system was utilized for anion impurityfree colloidal syntheses of semiconducting metal chalcogenide nanoparticles, an alternative to traditional metal salt based nanoparticle syntheses. Metals like Cu, In, Ga, Zn, Sn, Se were used in their elemental form to synthesize alkylammonium metal thiolate species using a propylamine and ethanedithiol solution. The thermal decomposition of these precursors was then studied using XRD and GC-MS analysis revealing a clean conversion of metal thiolates to metal chalcogenides along with volatile byproducts. Using this route, anion impurity-free, phase pure syntheses for binary In<sub>2</sub>S<sub>3</sub>, ternary CuInS<sub>2</sub> and quaternary Cu<sub>2</sub>ZnSnS<sub>4</sub> systems were demonstrated. Uniform metal alloying between In and Ga was also successfully achieved for the binary alloy (In<sub>x</sub>Ga<sub>1-x</sub>)<sub>2</sub>S<sub>3</sub> and the ternary alloy CIGS system, while chalcogen alloying with Se was demonstrated for the CISSe system. The success of heat-up, hot injection and microwave assisted solvothermal route for synthesizing phase pure material provided flexibility in experimental methods while the formation of different size, shape, and phase of nanoparticles via selective reaction parameters provided control over reaction products from these new precursor solutions. The applicability of this route was further explored by preparing precursor inks using metal chalcogenides instead of pure metals, which still avoid the use of any foreign impurity, to synthesize ternary metal chalcogenide nanoparticles of CIGS and AgInS<sub>2</sub>.

#### **Supporting Information**

Raman spectroscopy data of CIS nanoparticles, XRD data of indium sulfide particles with thiol variation, GC-MS data on the indium sulfide reaction mixture, XRD/TEM/STEM-EDS data on indium gallium sulfide particles, Raman/STEM-EDS/XRD/FTIR/<sup>1</sup>H-NMR data on CIGS nanoparticles, XRD/STEM-EDS data on CISSe nanoparticles, XRD/Raman/TEM data on CIGS nanoparticles from Cu<sub>2</sub>S precursor, TEM image of wurtzite phase CIGS nanoparticles.

#### Acknowledgment

The authors would like to acknowledge the funding support provided by the National Science Foundation under grant #1534691-DMR (DMREF) and grant #1735282-NRT (SFEWS). The authors would also like to acknowledge Jonathan Turnley and Aashish Rai for their help with nanoparticle synthesis experiments, Joseph Andler for his help with atomic force microscopy measurements, Prof. Daniel Flaherty from Department of Medicinal Chemistry and Molecular Pharmacology at Purdue University for allowing use of their microwave reactor and Prof. John Blendell from Department of Materials Engineering at Purdue University for allowing use of atomic force microscope.

#### References

- (1) Nakamura, M.; Yamaguchi, K.; Kimoto, Y.; Yasaki, Y.; Kato, T.; Sugimoto, H. Cd-Free Cu(In,Ga)(Se,S)<sub>2</sub> Thin-Film Solar Cell with a New World Record Efficacy of 23.35%. In *46th IEEE PVSC*, **2019**.
- Zhang, T.; Yang, Y.; Liu, D.; Tse, S. C.; Cao, W.; Feng, Z.; Chen, S.; Qian, L. High Efficiency Solution-Processed Thin-Film Cu(In,Ga)(Se,S)<sub>2</sub> Solar Cells. *Energy Environ. Sci.* **2016**, *9* (12), 3674–3681.
- (3) Wang, W.; Winkler, M. T.; Gunawan, O.; Gokmen, T.; Todorov, T. K.; Zhu, Y.; Mitzi, D. B. Device Characteristics of CZTSSe Thin-Film Solar Cells with 12.6% Efficiency. *Adv. Energy Mater.* **2014**, *4* (7), 1301465.
- (4) Uhl, A. R.; Katahara, J. K.; Hillhouse, H. W. Molecular-Ink Route to 13.0% Efficient Low-Bandgap CuIn(S,Se)<sub>2</sub> and 14.7% Efficient Cu(In,Ga)(S,Se)<sub>2</sub> Solar Cells. *Energy Environ. Sci.* **2016**, *9* (1), 130–134.
- (5) Clark, J. A.; Murray, A.; Lee, J. M.; Autrey, T. S.; Collord, A. D.; Hillhouse, H. W. Complexation Chemistry in N,N-Dimethylformamide-Based Molecular Inks for Chalcogenide Semiconductors and Photovoltaic Devices. *J. Am. Chem. Soc.* **2019**, *141* (1), 298–308.
- (6) Clark, J. A.; Uhl, A. R.; Martin, T. R.; Hillhouse, H. W. Evolution of Morphology and Composition during Annealing and Selenization in Solution-Processed Cu<sub>2</sub>ZnSn(S,Se)<sub>4</sub>. *Chem. Mater.* **2017**, *29* (21), 9328–9339.
- (7) Hossain, M. A.; Tianliang, Z.; Keat, L. K.; Xianglin, L.; Prabhakar, R. R.; Batabyal, S. K.; Mhaisalkar, S. G.; Wong, L. H. Synthesis of Cu(In,Ga)(S,Se)<sub>2</sub> Thin Films Using an Aqueous Spray-Pyrolysis Approach, and Their Solar Cell Efficiency of 10.5%. *J. Mater. Chem. A* **2015**, *3* (8), 4147–4154.
- (8) Zhang, R.; Szczepaniak, S. M.; Carter, N. J.; Handwerker, C. A.; Agrawal, R. A Versatile Solution Route to Efficient Cu<sub>2</sub>ZnSn(S,Se)<sub>4</sub> Thin-Film Solar Cells. *Chem. Mater.* **2015**, *27* (6), 2114–2120.
- (9) Zhao, X.; Lu, M.; Koeper, M. J.; Agrawal, R. Solution-Processed Sulfur Depleted Cu(In, Ga)Se<sub>2</sub> Solar Cells Synthesized from a Monoamine–dithiol Solvent Mixture. *J. Mater. Chem. A* **2016**, *4* (19), 7390–7397..
- (10) Zhang, R.; Cho, S.; Lim, D. G.; Hu, X.; Stach, E. A.; Handwerker, C. A.; Agrawal, R. Metal–metal Chalcogenide Molecular Precursors to Binary, Ternary, and Quaternary Metal Chalcogenide Thin Films for Electronic Devices. *Chem. Commun.* **2016**, *52* (28), 5007–5010.
- (11) Fan, Q.; Tian, Q.; Wang, H.; Zhao, F.; Kong, J.; Wu, S. Regulating the Starting Location of Front-Gradient

- Enabled Highly Efficient Cu(In,Ga)Se<sub>2</sub> Solar Cells *via* a Facile Thiol–amine Solution Approach. *J. Mater. Chem. A* **2018**, *6* (9), 4095–4101.
- (12) Zhao, D.; Tian, Q.; Zhou, Z.; Wang, G.; Meng, Y.; Kou, D.; Zhou, W.; Pan, D.; Wu, S. Solution-Deposited Pure Selenide CIGSe Solar Cells from Elemental Cu, In, Ga, and Se. *J. Mater. Chem. A* **2015**, *3* (38), 19263–19267.
- (13) McLeod, S. M.; Hages, C. J.; Carter, N. J.; Agrawal, R. Synthesis and Characterization of 15% Efficient CIGSSe Solar Cells from Nanoparticle Inks. *Prog. Photovoltaics Res. Appl.* **2015**, *23* (11), 1550–1556.
- (14) Larramona, G.; Levcenko, S.; Bourdais, S.; Jacob, A.; Choné, C.; Delatouche, B.; Moisan, C.; Just, J.; Unold, T.; Dennler, G. Fine-Tuning the Sn Content in CZTSSe Thin Films to Achieve 10.8% Solar Cell Efficiency from Spray-Deposited Water-Ethanol-Based Colloidal Inks. Adv. Energy Mater. 2015, 5 (24), 1–10
- (15) Miskin, C. K.; Yang, W.-C.; Hages, C. J.; Carter, N. J.; Joglekar, C. S.; Stach, E. A.; Agrawal, R. 9.0% Efficient Cu<sub>2</sub>ZnSn(S,Se)<sub>4</sub> Solar Cells from Selenized Nanoparticle Inks. *Prog. Photovoltaics Res. Appl.* 2015, 23 (5), 654–659.
- (16) Hages, C. J.; Koeper, M. J.; Miskin, C. K.; Brew, K. W.; Agrawal, R. Controlled Grain Growth for High Performance Nanoparticle-Based Kesterite Solar Cells. *Chem. Mater.* 2016, 28 (21), 7703–7714.
- (17) Barbé, J.; Eid, J.; Ahlswede, E.; Spiering, S.; Powalla, M.; Agrawal, R.; Del Gobbo, S. Inkjet Printed Cu(In,Ga)S<sub>2</sub> Nanoparticles for Low-Cost Solar Cells. *J. Nanoparticle Res.* **2016**, *18* (12), 379.
- (18) Guo, Q.; Kim, S. J.; Kar, M.; Shafarman, W. N.; Birkmire, R. W.; Stach, E. A.; Agrawal, R.; Hillhouse, H. W. Development of CulnSe<sub>2</sub> Nanocrystal and Nanoring Inks for Low-Cost Solar Cells. *Nano Lett.* **2008**, *8* (9), 2982–2987.
- (19) Guo, Q.; Hillhouse, H. W.; Agrawal, R. Synthesis of Cu<sub>2</sub>ZnSnS<sub>4</sub> Nanocrystal Ink and Its Use for Solar Cells. J. Am. Chem. Soc. 2009, 131 (33), 11672–11673.
- (20) Hages, C. J.; Agrawal, R. Synthesis of CZTSSe Thin Films from Nanocrystal Inks. In *Copper Zinc Tin Sulfide-Based Thin-Film Solar Cells*; Ito, K., Ed.; John Wiley & Sons Ltd: Chichester, UK, **2015**, 239–270.
- (21) Coughlan, C.; Ibáñez, M.; Dobrozhan, O.; Singh, A.; Cabot, A.; Ryan, K. M. Compound Copper Chalcogenide Nanocrystals. *Chem. Rev.* **2017**, *117* (9), 5865–6109.
- (22) Liu, Y.; Liu, M.; Yin, D.; Qiao, L.; Fu, Z.; Swihart, M. T. Selective Cation Incorporation into Copper Sulfide Based Nanoheterostructures. *ACS Nano* **2018**, *12* (8), 7803–7811.
- Liu, Y.; Liu, M.; Yin, D.; Wei, W.; Prasad, P. N.; Swihart, M. T. Kuramite Cu<sub>3</sub>SnS<sub>4</sub> and Mohite Cu<sub>2</sub>SnS<sub>3</sub> Nanoplatelet Synthesis Using Covellite CuS Templates with Sn(II) and Sn(IV) Sources. *Chem. Mater.* **2017**, 29 (8), 3555–3562.
- Houck, D. W.; Nandu, S. V.; Siegler, T. D.; Korgel, B. A. CuGaSe<sub>2</sub> and CuIn<sub>X</sub>Ga<sub>1-X</sub>Se<sub>2</sub> Nanocrystals with Sphalerite or Wurtzite Phase for Optoelectronic Applications . *ACS Appl. Nano Mater.* **2019**, *2* (7), 4673–4680.
- (25) Kar, M.; Agrawal, R.; Hillhouse, H. W. Formation Pathway of CuInSe<sub>2</sub> Nanocrystals for Solar Cells. *J. Am. Chem. Soc.* **2011**, *133* (43), 17239–17247.
- (26) Lany, S.; Yu-Jun Zhao; Persson, C.; Zunger, A. N-Type Doping Principles for Doping CuInSe<sub>2</sub> and CuGaSe<sub>2</sub> with Cl, Br, I, Mg, Zn, and Cd. In *31st IEEE PVSC*, *2005*, 343–346.
- (27) Murria, P.; Miskin, C. K.; Boyne, R.; Cain, L. T.; Yerabolu, R.; Zhang, R.; Wegener, E. C.; Miller, J. T.; Kenttämaa, H. I.; Agrawal, R. Speciation of CuCl and CuCl<sub>2</sub> Thiol-Amine Solutions and Characterization of Resulting Films: Implications for Semiconductor Device Fabrication. *Inorg. Chem.* **2017**, *56* (23), 14396–14407.
- (28) Selishcheva, E.; Parisi, J.; Kolny-Olesiak, J. Copper-Assisted Shape Control in Colloidal Synthesis of Indium Oxide Nanoparticles. *J. Nanoparticle Res.* **2012**, *14* (2), 711.
- (29) Cavallari, N.; Pattini, F.; Rampino, S.; Annoni, F.; Barozzi, M.; Bronzoni, M.; Gilioli, E.; Gombia, E.; Maragliano, C.; Mazzer, M.; et al. Low Temperature Deposition of Bifacial CIGS Solar Cells on Al-Doped Zinc Oxide Back Contacts. *Appl. Surf. Sci.* **2017**, *412*, 52–57.
- (30) Boles, M. A.; Ling, D.; Hyeon, T.; Talapin, D. V. The Surface Science of Nanocrystals. *Nat. Mater.* **2016**, *15* (2), 141–153.
- (31) Rath, T.; Edler, M.; Haas, W.; Fischereder, A.; Moscher, S.; Schenk, A.; Trattnig, R.; Sezen, M.; Mauthner, G.; Pein, A.; et al. A Direct Route towards Polymer/copper Indium Sulfide Nanocomposite Solar Cells. *Adv. Energy Mater.* **2011**, *1* (6), 1046–1050.
- Wang, G.; Wang, S.; Cui, Y.; Pan, D. A Novel and Versatile Strategy to Prepare Metal-Organic Molecular Precursor Solutions and Its Application in Cu(In,Ga)(S,Se)<sub>2</sub> Solar Cells. *Chem. Mater.* **2012**, *24* (20), 3993–3997.

- (33) Chesman, A. S. R.; Van Embden, J.; Duffy, N. W.; Webster, N. A. S.; Jasieniak, J. J. In Situ Formation of Reactive Sulfide Precursors in the One-Pot, Multigram Synthesis of Cu<sub>2</sub>ZnSnS<sub>4</sub> Nanocrystals. *Cryst. Growth Des.* **2013**, *13* (4), 1712–1720.
- van Embden, J.; Chesman, A. S. R.; Jasieniak, J. J. The Heat-Up Synthesis of Colloidal Nanocrystals. *Chem. Mater.* **2015**, *27* (7), 2246–2285.
- Jiang, Y.; Wu, Y.; Mo, X.; Yu, W.; Xie, Y.; Qian, Y. Elemental Solvothermal Reaction to Produce Ternary Semiconductor CuInE<sub>2</sub> (E = S, Se) Nanorods. *Inorg. Chem.* **2000**, *39* (14), 2964–2965.
- (36) Chun, Y.-G.; Kim, K.-H.; Yoon, K.-H. Synthesis of CuInGaSe<sub>2</sub> Nanoparticles by Solvothermal Route. *Thin Solid Films* **2005**, *480–481*, 46–49.
- (37) Webber, D. H.; Buckley, J. J.; Antunez, P. D.; Brutchey, R. L. Facile Dissolution of Selenium and Tellurium in a Thiol–amine Solvent Mixture under Ambient Conditions. *Chem. Sci.* **2014**, *5* (6), 2498.
- (38) Walker, B. C.; Agrawal, R. Contamination-Free Solutions of Selenium in Amines for Nanoparticle Synthesis. *Chem. Commun.* **2014**, *50* (61), 8331–8334.
- (39) Liu, Y.; Yao, D.; Shen, L.; Zhang, H.; Zhang, X.; Yang, B. Alkylthiol-Enabled Se Powder Dissolution in Oleylamine at Room Temperature for the Phosphine-Free Synthesis of Copper-Based Quaternary Selenide Nanocrystals. *J. Am. Chem. Soc.* **2012**, *134* (17), 7207–7210.
- (40) Miskin, C. K.; Deshmukh, S. D.; Vasiraju, V.; Bock, K.; Mittal, G.; Dubois-Camacho, A.; Vaddiraju, S.; Agrawal, R. Lead Chalcogenide Nanoparticles and Their Size-Controlled Self-Assemblies for Thermoelectric and Photovoltaic Applications. *ACS Appl. Nano Mater.* **2019**, *2* (3), 1242–1252.
- (41) Agrawal, R.; Zhang, R; Walker, B. C.; Handwerker, C. Homogeneous Precursor Formation Method and Device Thereof. US 9,738,799 B2, August 12, **2015**.
- (42) Zhao, X.; Deshmukh, S. D.; Rokke, D. J.; Zhang, G.; Wu, Z.; Miller, J. T.; Agrawal, R. Investigating Chemistry of Metal Dissolution in Amine–Thiol Mixtures and Exploiting It toward Benign Ink Formulation for Metal Chalcogenide Thin Films. *Chem. Mater.* **2019**, *31* (15), 5674–5682.
- (43) Dierick, R.; Van den Broeck, F.; De Nolf, K.; Zhao, Q.; Vantomme, A.; Martins, J. C.; Hens, Z. Surface Chemistry of CuInS<sub>2</sub> Colloidal Nanocrystals, Tight Binding of L-Type Ligands. *Chem. Mater.* **2014**, *26* (20), 5950–5957.
- (44) Rokke, D.; Deshmukh, S. D.; Agrawal, R. A Novel Approach to Amine-Thiol Molecular Precursors for Fabrication of High Efficiency Thin Film CISSe/CIGSSe Devices. In *46th IEEE PVSC*, **2019**.
- (45) Dutta, D. P.; Sharma, G.; Tyagi, A. K.; Kulshreshtha, S. K. Gallium Sulfide and Indium Sulfide Nanoparticles from Complex Precursors: Synthesis and Characterization. *Mater. Sci. Eng. B* **2007**, *138* (1), 60–64
- (46) Rau, U.; Schock, H. W. Cu(In,Ga)Se<sub>2</sub> Thin-Film Solar Cells. In *Solar Cells*; Elsevier, **2013**, 261–304.
- (47) Carter, N. J.; Yang, W. C.; Miskin, C. K.; Hages, C. J.; Stach, E. A.; Agrawal, R. Cu<sub>2</sub>ZnSn(S,Se)<sub>4</sub> Solar Cells from Inks of Heterogeneous Cu-Zn-Sn-S Nanocrystals. *Sol. Energy Mater. Sol. Cells* **2014**, *123*, 189–196.
- (48) Yang, W.-C.; Miskin, C. K.; Carter, N. J.; Agrawal, R.; Stach, E. A. Compositional Inhomogeneity of Multinary Semiconductor Nanoparticles: A Case Study of Cu<sub>2</sub>ZnSnS<sub>4</sub>. Chem. Mater. 2014, 26 (24), 6955-6962
- (49) Yu, X.; Cheng, S.; Yan, Q.; Yu, J.; Qiu, W.; Zhou, Z.; Zheng, Q.; Wu, S. Efficient (Cu<sub>1-x</sub>Ag<sub>x</sub>)<sub>2</sub>ZnSn(S,Se)<sub>4</sub> Solar Cells on Flexible Mo Foils. *RSC Adv.* **2018**, *8* (49), 27686–27694.
- (50) Liu, Z.; Tang, K.; Wang, D.; Wang, L.; Hao, Q. Facile Synthesis of AgInS<sub>2</sub> Hierarchical Flowerlike Nanoarchitectures Composed of Ultrathin Nanowires. *Nanoscale* **2013**, *5* (4), 1570–1575.

## **Supporting Information**

# **Versatile Colloidal Syntheses of Metal Chalcogenide Nanoparticles from Elemental Precursors using Amine-Thiol Chemistry**

Swapnil D. Deshmukh, † Ryan G. Ellis, † Dwi S. Sutandar, David J. Rokke, and Rakesh Agrawal\*

Davidson School of Chemical Engineering, Purdue University, West Lafayette, IN 47907, USA

<sup>†</sup> These authors contributed equally

<sup>\*</sup>Corresponding author: agrawalr@purdue.edu

## **CIS Nanoparticle Synthesis:**

CIS nanoparticles synthesized from various experimental methods including the hot injection, one pot heat up and microwave assisted solvothermal routes yield phase pure material without any presence of binary as can be seen from Raman analysis.

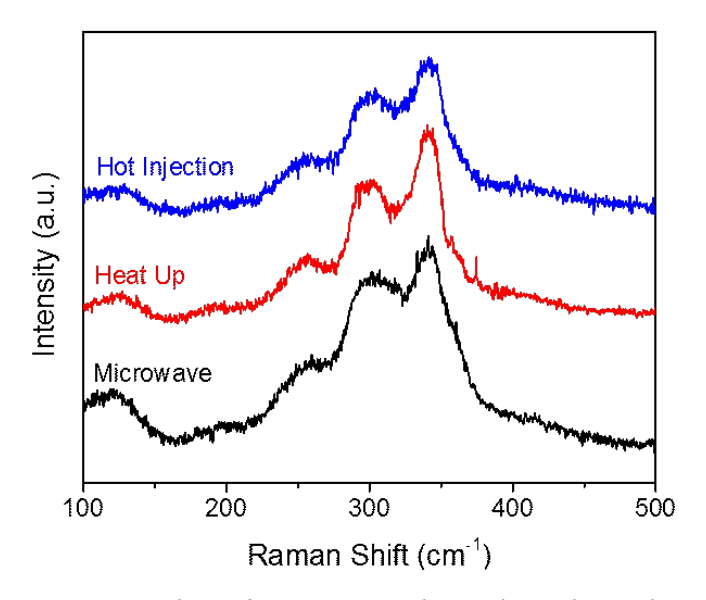


Figure S1. Raman spectroscopy analysis of CIS nanoparticles synthesized using hot injection, heat up and microwave assisted solvothermal reaction.

#### **Effect of Thiol on Indium Sulfide Particles:**

The evolution of amorphous trigonal indium sulfide to more crystalline tetragonal indium sulfide as a function of time could be related to the amount of thiol present in the reaction solution as a function of time. To verify this hypothesis, reactions were carried out for 60 min with varying quantity of thiol in the starting reaction solution. Although both the reactions resulted in mixture of amorphous trigonal indium sulfide and crystalline tetragonal indium sulfide, the reaction with reduced thiol quantity resulted in higher fraction of crystalline material as compare to reaction with excess thiol, supporting the hypothesis for thiol effect.

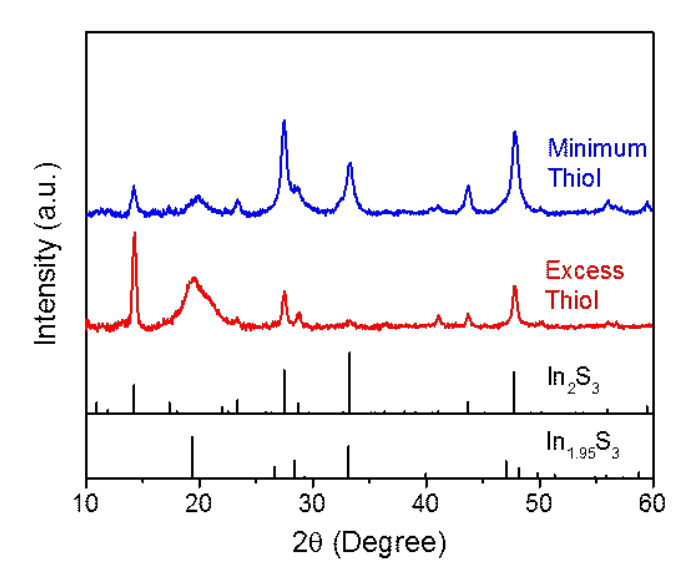


Figure S2. XRD analysis of indium sulfide particles synthesized using hot injection route for 60 min reactions with different thiol quantities. (Tetragonal phase In<sub>2</sub>S<sub>3</sub> and trigonal phase In<sub>1.95</sub>S<sub>3</sub> standards with ICSD collection code 151645 and 244280 respectively)

## GC-MS Analysis of Indium Sulfide Reaction:

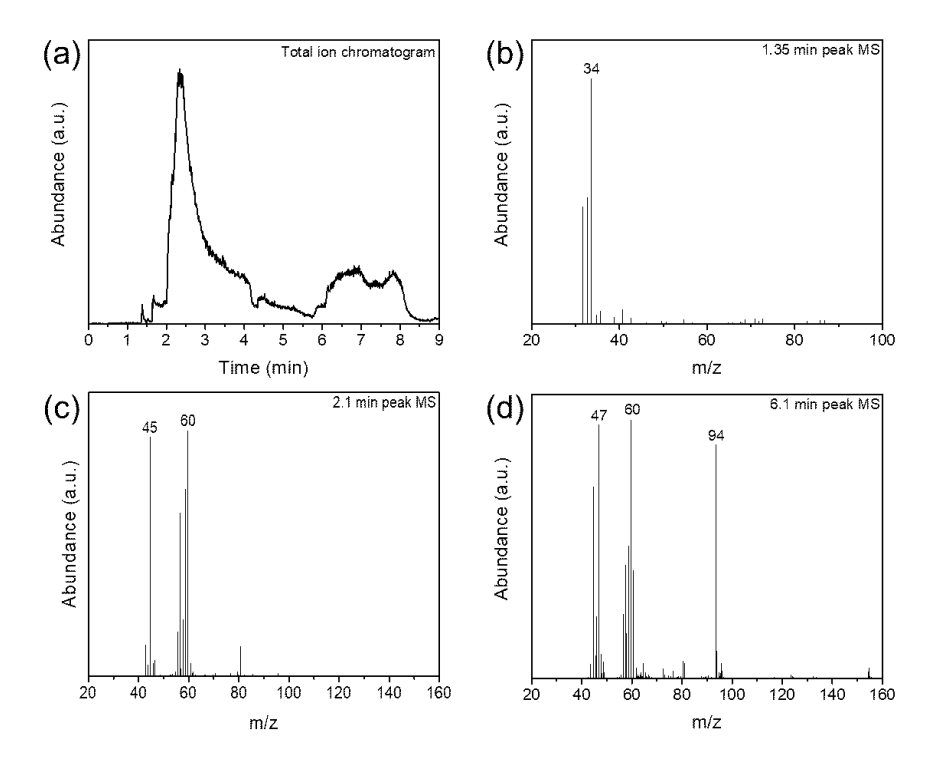


Figure S3. (a) Total ion chromatogram collected for indium-octylamine-ethanedithiol solution. Analyzed mass spectrum of isolated peak at elution time of (b) 1.35 min, (c) 2.1 min and (d) 6.1 min.

## **Cupper Sulfide Synthesis:**

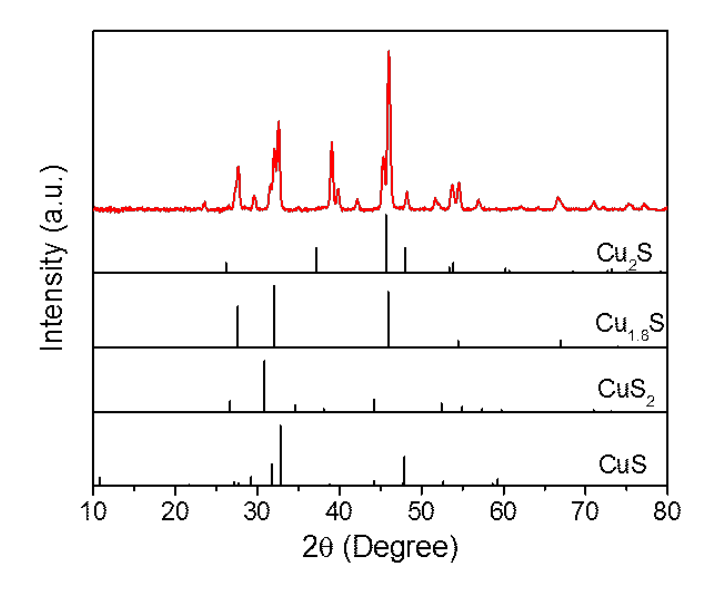


Figure S4. XRD analysis of nanoparticles synthesized via hot injection of Cu-PA-EDT ink in OLA showing formation of different phases of copper sulfides. (Cu<sub>2</sub>S, Cu<sub>1.8</sub>S, CuS<sub>2</sub> and CuS standards with ICSD collection code 200988, 95395, 100510 and 61793 respectively)

### **In-Ga Alloying:**

Increasing gallium fraction in In-Ga sulfide resulted in reduced crystallinity of the particles as can be seen from XRD pattern below. The peak around 20° is shifted towards higher angles with increasing Ga fractions, suggesting possible incorporation of Ga into indium sulfide. The extent and uniformity of this alloying is further confirmed by performing STEM-EDS analysis on particles.

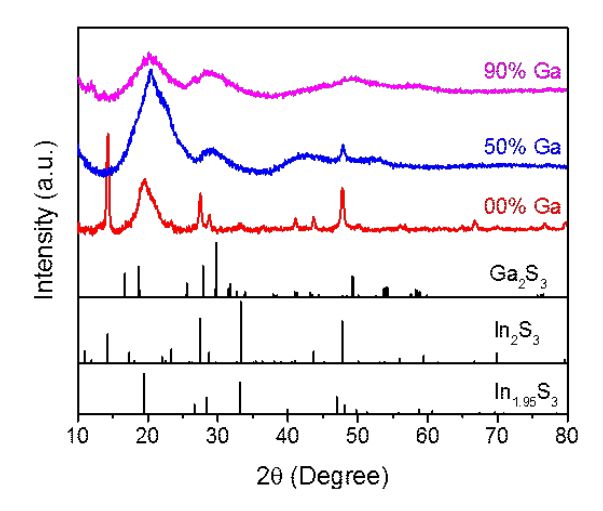


Figure S5. XRD analysis of indium-gallium sulfide particles synthesized using hot injection route with different gallium fractions. (Tetragonal phase  $In_2S_3$ , trigonal phase  $In_1.95S_3$  and  $Ga_2S_3$  standards with ICSD collection code 151645, 244280 and 409550 respectively)

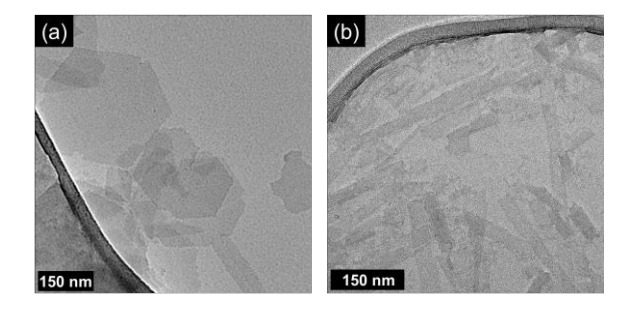


Figure S6. TEM images of indium-gallium sulfide nanostructures synthesized using hot injection with (a) 50% Ga and (b) 90% Ga fraction

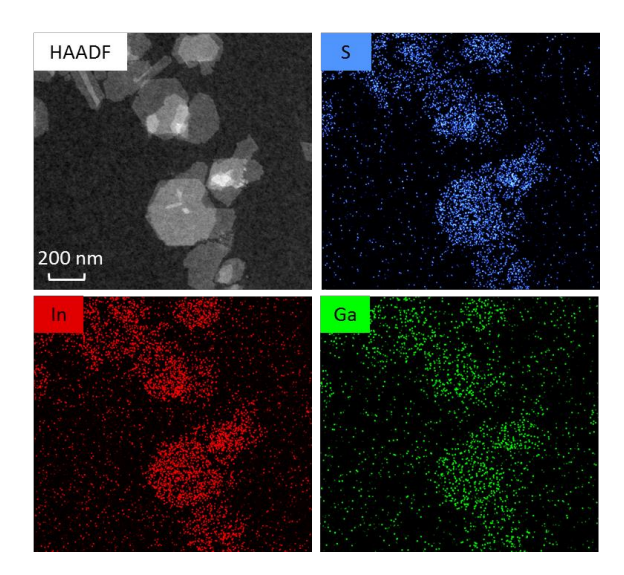


Figure S7. STEM-EDS elemental mapping of indium-gallium sulfide nanostructure containing 50% Ga showing uniformity of alloying within single particles as well as between multiple particles.

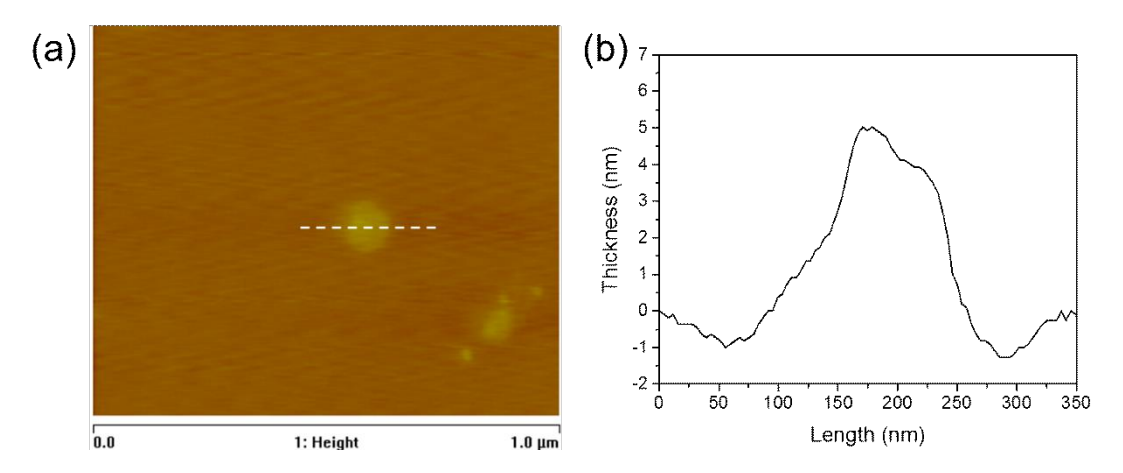


Figure S8. Atomic force microscopy on indium gallium sulfide nanostructure containing 50% Ga. (a) AFM image of the nanostructure (b) Plot showing thickness measurement of the nanostructure along the white dash line.

#### **CIGS Nanoparticle Synthesis:**

CIGS nanoparticle synthesis performed via one pot heat up route show absence of any binary formation (based on Raman analysis) for aliquots collected at various temperature during the course of heat up process. As can be seen from Figure S9, the A1 mode of CIS nanoparticles at 294 cm<sup>-1</sup> shifts toward higher Raman shift of around 298 cm<sup>-1</sup>, suggesting incorporation of Ga with increasing reaction temperature. Ga incorporation and elemental uniformity of CIGS particles is further confirmed via STEM-EDS analysis (Figure S10), while the particle surface is analyzed using FTIR (Figure 12a) and  $^{1}$ H-NMR technique (Figure 12b), confirming the presence of oleylamine as ligand. The extra NMR peaks at  $\delta$  of 4.03 ppm and 1.21 ppm corresponds to isopropyl alcohol used for washing nanoparticles while peak at  $\delta$  of 4.54 ppm corresponds to ethylene carbonate, which was used as an internal 1H-NMR standard.

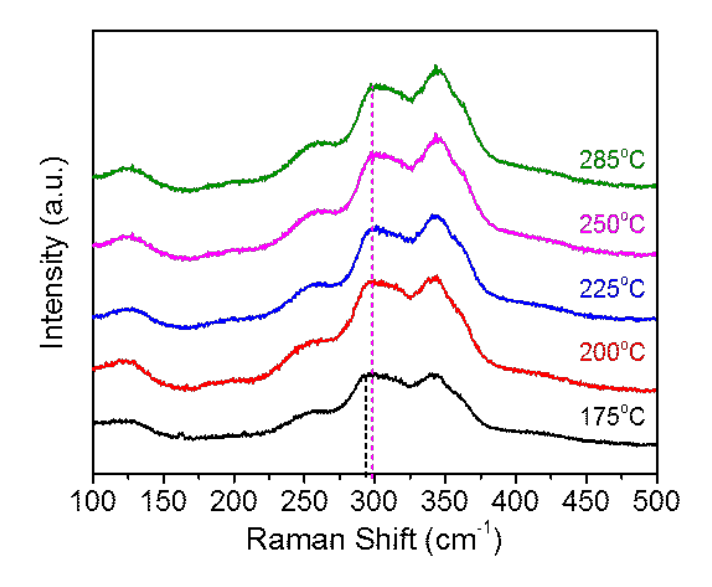


Figure S9. Raman analysis of CIGS nanoparticles during heat up process, showing incorporation of gallium in CIS structure as a function of temperature.

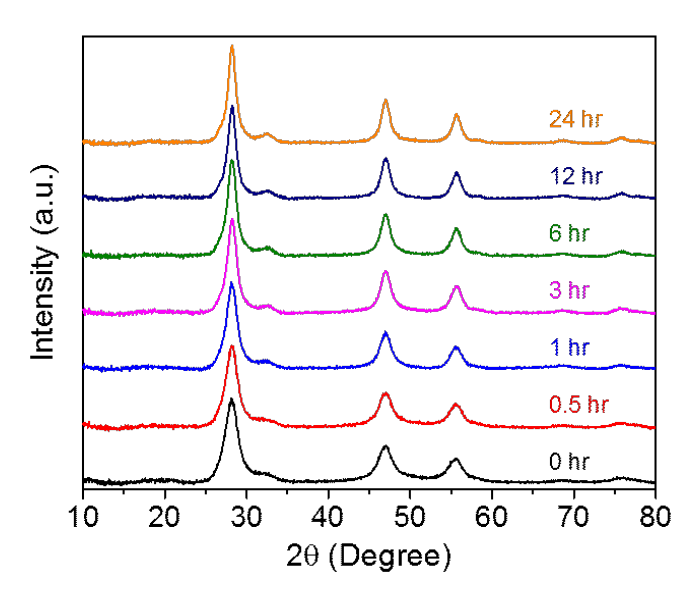


Figure S10. XRD analysis of CIGS nanoparticles synthesized using heat up route with different time aliquots showing reduced FWHM of peaks corresponding to increased particle size.

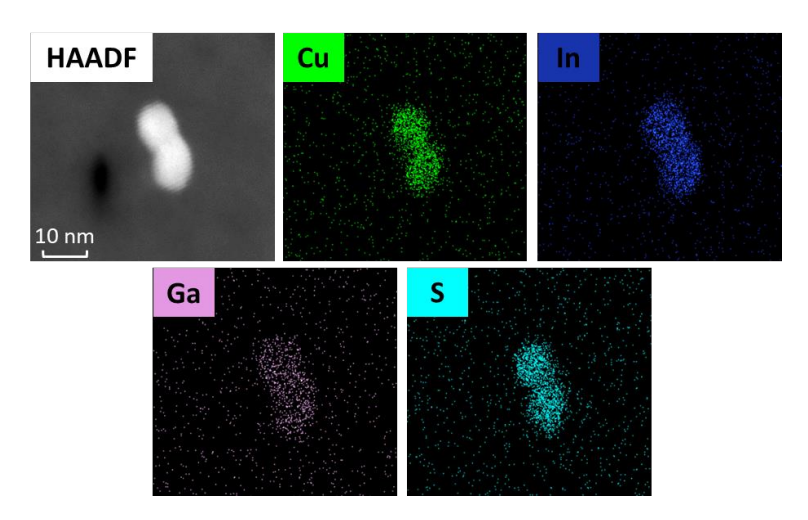


Figure S11. STEM-EDS elemental mapping of CIGS nanoparticles containing Ga/(Ga+In) of 0.3, showing elemental uniformity within single particles as well as between multiple particles.

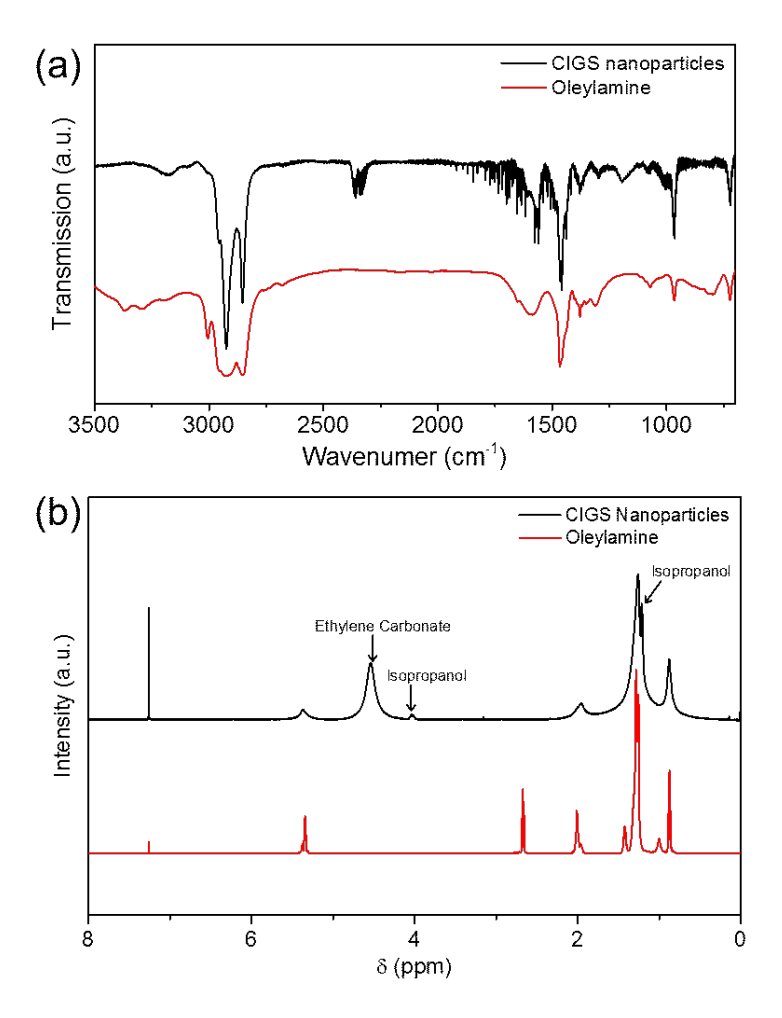


Figure S12. (a) FTIR analysis and (b) <sup>1</sup>H-NMR analysis of CIGS nanoparticles synthesized using heat up route confirming the presence of oleylamine on particle surface.

## **CISSe Nanoparticle Synthesis:**

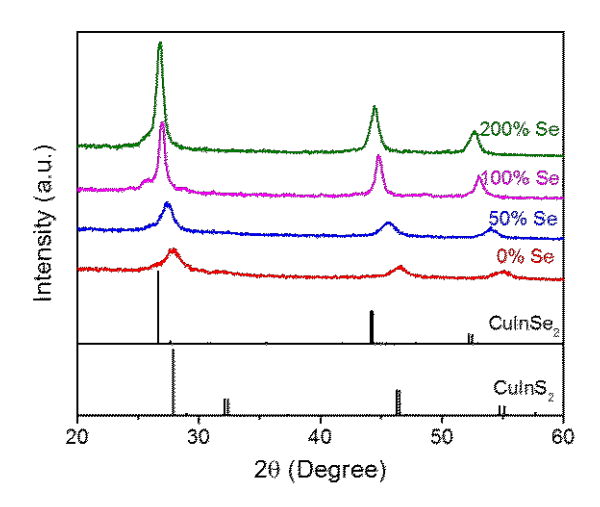


Figure S13. XRD analysis on CISSe nanoparticles as a function of Se quantity. (Chalcopyrite phase CIS and CISe standards with ICSD collection code 186714 and 73351 respectively)

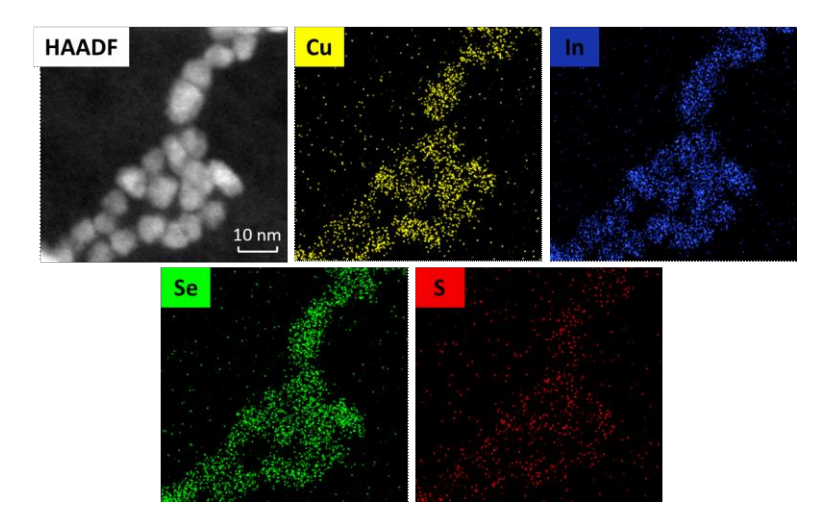


Figure S14. STEM-EDS elemental mapping of CISSe nanoparticles synthesized with reaction containing Se/(Cu+In) ratio of 2, showing elemental uniformity within single particles as well as between multiple particles.

### **CZTS** Nanoparticle Synthesis suing heat up process:

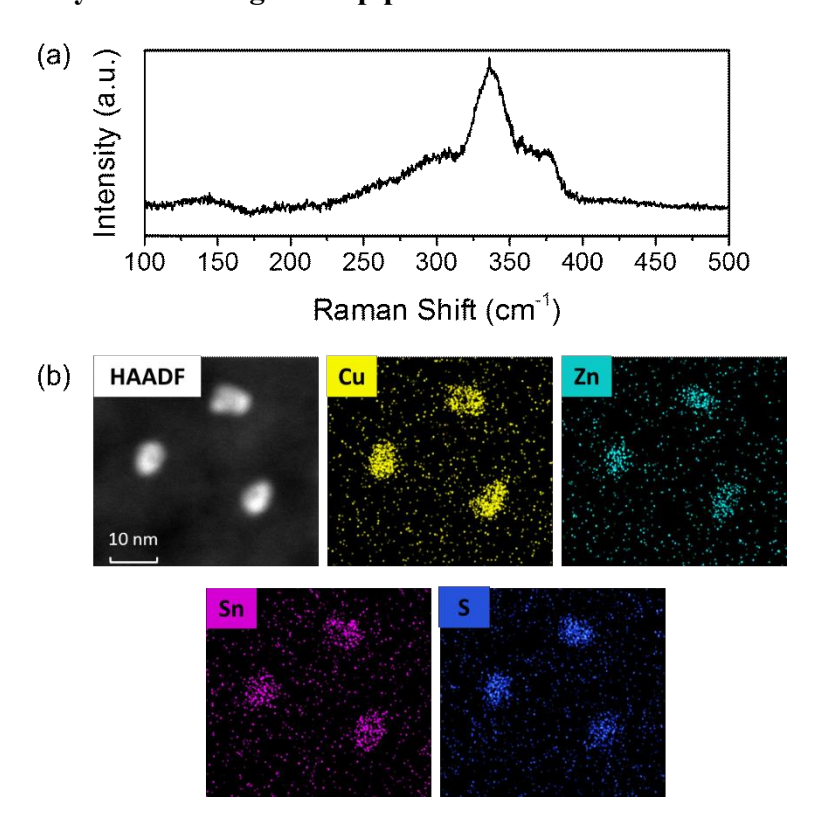


Figure S15. (a) Raman Spectroscopy analysis and (b) STEM-EDS elemental mapping of CZTS nanoparticles.

## CIGS Nanoparticle Synthesis from Cu<sub>2</sub>S Precursor:

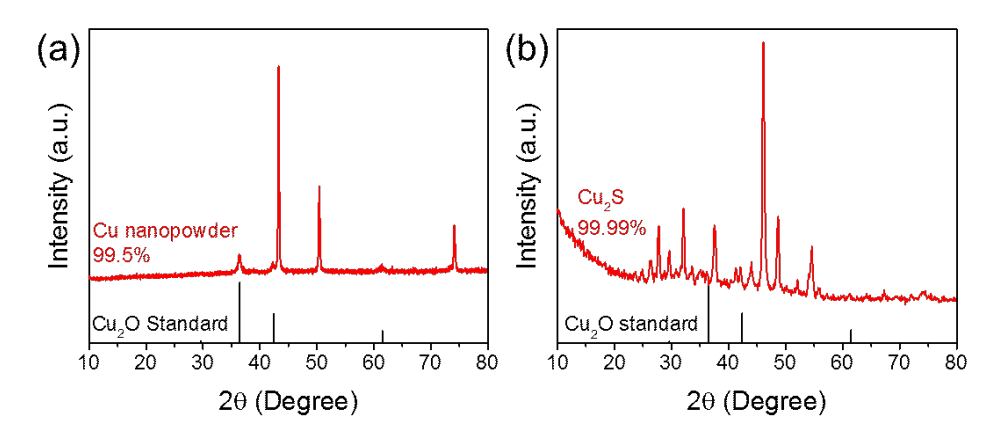


Figure S16. XRD analysis on as received (a) 99.5% pure Cu nanopowder showing presence of Cu<sub>2</sub>O material and (b) 99.99% pure Cu<sub>2</sub>S powder showing absence of Cu<sub>2</sub>O materials.

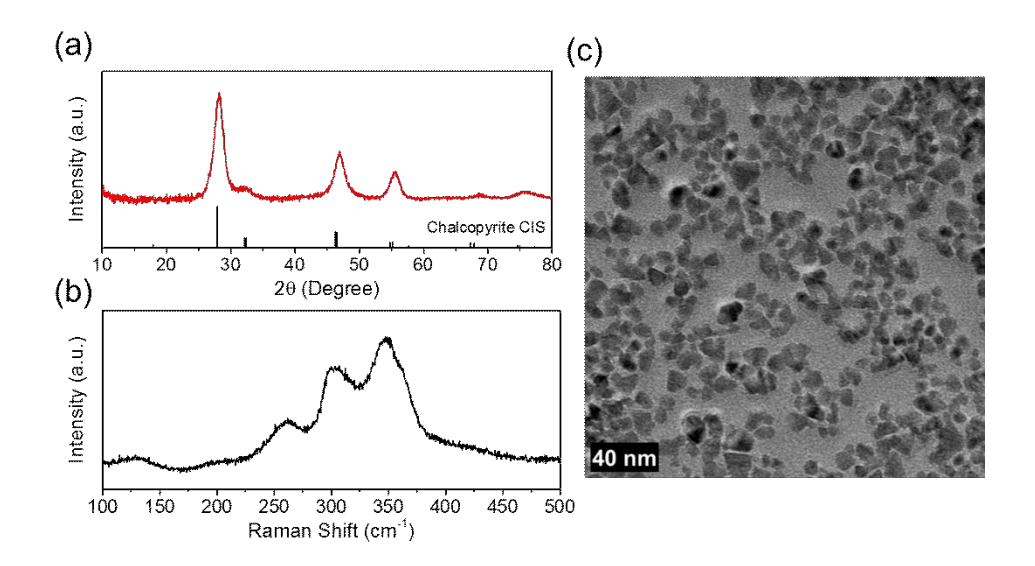


Figure S17. (a) XRD analysis, (b) Raman analysis and (c) TEM image of CIGS nanoparticles synthesized via heat up route using Cu<sub>2</sub>S precursor instead of elemental Cu. (Chalcopyrite phase CIS standards with ICSD collection code 186714)

## **Wurtzite Phase CIGS Nanoparticle Synthesis:**

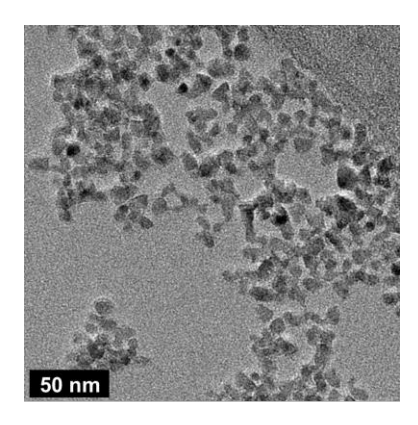


Figure S18. TEM images of wurtzite phase CIGS nanoparticles synthesized via heat up route with faster heating rate and 3 hours of reaction time